



**HAL**  
open science

## Postcranial anatomy of the extinct terrestrial sloth *Simomylodon uccasamamensis* (Xenarthra, Mylodontidae) from the Pliocene of the Bolivian Altiplano, and its evolutionary implications

Alberto Boscaini, Néstor Toledo, Bernardino Mamani Quispe, Rubén Andrade Flores, Marcos Fernández-monescillo, Laurent Marivaux, Pierre-Olivier Antoine, Philippe Münch, Timothy Gaudin, François Pujos

### ► To cite this version:

Alberto Boscaini, Néstor Toledo, Bernardino Mamani Quispe, Rubén Andrade Flores, Marcos Fernández-monescillo, et al.. Postcranial anatomy of the extinct terrestrial sloth *Simomylodon uccasamamensis* (Xenarthra, Mylodontidae) from the Pliocene of the Bolivian Altiplano, and its evolutionary implications. *Papers in Palaeontology*, 2021, 7 (3), pp.1557-1583. 10.1002/spp2.1353 . hal-03136053

**HAL Id: hal-03136053**

**<https://hal.umontpellier.fr/hal-03136053>**

Submitted on 9 Feb 2021

**HAL** is a multi-disciplinary open access archive for the deposit and dissemination of scientific research documents, whether they are published or not. The documents may come from teaching and research institutions in France or abroad, or from public or private research centers.

L'archive ouverte pluridisciplinaire **HAL**, est destinée au dépôt et à la diffusion de documents scientifiques de niveau recherche, publiés ou non, émanant des établissements d'enseignement et de recherche français ou étrangers, des laboratoires publics ou privés.



**POSTCRANIAL ANATOMY OF THE EXTINCT TERRESTRIAL SLOTH *SIMOMYLODON UCCASAMAMENSIS* (XENARTHRA: MYLODONTIDAE) FROM THE PLIOCENE OF THE BOLIVIAN ALTIPLANO AND ITS EVOLUTIONARY IMPLICATIONS**

Journal:	<i>Palaeontology</i>
Manuscript ID	PALA-06-20-4813-OA.R1
Manuscript Type:	Original Article
Date Submitted by the Author:	n/a
Complete List of Authors:	<p>Boscaini, Alberto; Universidad Nacional de la Plata, Toledo, Nestor; Museo de La Plata, División Paleontología de Vertebrados Mamani Quispe, Bernardino; Museo Nacional de Historia Natural de Bolivia</p> <p>Andrade Flores, Rubén ; Museo Nacional de Historia Natural de Bolivia</p> <p>Fernández-Monescillo, Marcos; Universidad Nacional de Córdoba Facultad de Ciencias Exactas Físicas y Naturales</p> <p>Marivaux, Laurent; Institut des sciences de l'évolution, Paleontology Antoine, Pierre-Olivier; ISEM CC064</p> <p>Münch, Philippe; Géosciences Montpellier, Université de Montpellier, CNRS</p> <p>Gaudin, Timothy; University of Tennessee at Chattanooga, Department of Biological and Environmental Sciences</p> <p>Pujos, François; Instituto Argentino de Nivología, Glaciología y Ciencias Ambientales, CCT-CONICET-Mendoza</p>
Key words:	anatomy, extinct sloth, evolution, Mylodontinae, postcranium, skeleton

SCHOLARONE™  
Manuscripts

1  
2  
3 POSTCRANIAL ANATOMY OF THE EXTINCT TERRESTRIAL SLOTH  
4  
5  
6 *SIMOMYLODON UCCASAMAMENSIS* (XENARTHRA: MYLODONTIDAE)  
7  
8  
9 FROM THE PLIOCENE OF THE BOLIVIAN ALTIPLANO AND ITS  
10  
11  
12 EVOLUTIONARY IMPLICATIONS  
13  
14  
15

16 by ALBERTO BOSCAINI<sup>1,2\*</sup>, NÉSTOR TOLEDO<sup>1</sup>, BERNARDINO MAMANI QUISPE<sup>3</sup>,  
17  
18 RUBÉN ANDRADE FLORES<sup>3</sup>, MARCOS FERNÁNDEZ-MONESCILLO<sup>4</sup>, LAURENT  
19  
20 MARIVAUX<sup>5</sup>, PIERRE-OLIVIER ANTOINE<sup>5</sup>, PHILIPPE MÜNCH<sup>6</sup>, TIMOTHY J.  
21  
22 GAUDIN<sup>7</sup> and FRANÇOIS PUJOS<sup>8</sup>  
23  
24

25 <sup>1</sup>CONICET, División Paleontología Vertebrados, Museo de La Plata, Unidades de Investigación Anexo Museo,  
26  
27 FCNyM, Calle 60 y 122, 1900 La Plata, Argentina; e-mails: [alberto.boscaini@gmail.com](mailto:alberto.boscaini@gmail.com)

28  
29 (<https://orcid.org/0000-0002-8666-9340>); [ntoledo@fcnym.unlp.edu.ar](mailto:ntoledo@fcnym.unlp.edu.ar) ([https://orcid.org/0000-0002-6833-](https://orcid.org/0000-0002-6833-3165)  
30  
31 [3165](https://orcid.org/0000-0002-6833-3165))  
32

33 <sup>2</sup>*Current address*: Instituto de Ecología, Genética y Evolución de Buenos Aires (IEGEB – CONICET). DEGE,  
34  
35 Facultad de Ciencias Exactas y Naturales, Universidad de Buenos Aires, Int. Guiraldes 2160, Buenos Aires,  
36  
37 Argentina.  
38

39 <sup>3</sup>Departamento de Paleontología, Museo Nacional de Historia Natural de Bolivia, Calle 26 s/n, Cota Cota, La  
40  
41 Paz, Bolivia; e-mails: [bmamaniq@hotmail.com](mailto:bmamaniq@hotmail.com); [randradeflores@gmail.com](mailto:randradeflores@gmail.com)  
42

43 <sup>4</sup>Museo de Paleontología, Facultad de Ciencias Exactas, Físicas y Naturales, Universidad Nacional de Córdoba,  
44  
45 Vélez Sarsfield 249, X5000JJC, Córdoba, Argentina; e-mail: [mfernandezmonescillo@gmail.com](mailto:mfernandezmonescillo@gmail.com)  
46  
47 (<https://orcid.org/0000-0002-0698-1909>)  
48

49 <sup>5</sup>Laboratoire de Paléontologie, Institut des Sciences de l'Évolution de Montpellier (ISE-M, UMR 5554,  
50  
51 CNRS/UM/IRD/EPHE), c.c. 64, Université de Montpellier (UM), Place Eugène Bataillon, 34095 Montpellier  
52  
53 Cedex 05, France ; e-mails: [laurent.marivaux@umontpellier.fr](mailto:laurent.marivaux@umontpellier.fr) (<https://orcid.org/0000-0002-2882-0874>); [pierre-](mailto:pierre-olivier.antoine@umontpellier.fr)  
54  
55 [olivier.antoine@umontpellier.fr](mailto:pierre-olivier.antoine@umontpellier.fr) (<https://orcid.org/0000-0001-9122-1818>)  
56

57 <sup>6</sup>Géosciences Montpellier (UMR 5243, CNRS/UM/Université des Antilles), c.c. 060, Université de Montpellier  
58  
59 (UM), Place Eugène Bataillon, 34095 Montpellier Cedex 05, France ; e-mail : [philippe.munch@umontpellier.fr](mailto:philippe.munch@umontpellier.fr)  
60  
(<https://orcid.org/0000-0003-4616-8039>)

1  
2  
3 <sup>7</sup>Department of Biology, Geology, and Environmental Science, University of Tennessee at Chattanooga, 615  
4 McCallie Ave, Chattanooga TN, 37403-2598, USA; e-mail: [Timothy-Gaudin@utc.edu](mailto:Timothy-Gaudin@utc.edu) ([https://orcid.org/0000-](https://orcid.org/0000-0003-0392-5001)  
5 [0003-0392-5001](https://orcid.org/0003-0392-5001))  
6  
7

8  
9 <sup>8</sup>Instituto Argentino de Nivología, Glaciología y Ciencias Ambientales (IANIGLA), CCT-CONICET-Mendoza,  
10 Avda. Ruiz Leal s/n, Parque Gral. San Martín, 5500 Mendoza, Argentina; e-mail: [fpujos@mendoza-](mailto:fpujos@mendoza-<br/>11 conicet.gob.ar)  
12 [conicet.gob.ar](https://orcid.org/0000-0002-6267-3927) (<https://orcid.org/0000-0002-6267-3927>)  
13  
14

15 \*Corresponding author  
16  
17  
18

19 **Abstract:** Extinct terrestrial sloths are common elements of the late Cenozoic South  
20 American fossil record. Among them, Mylodontinae species were particularly abundant in  
21 the Americas throughout the Pleistocene epoch, and their anatomy is relatively well known.  
22 In contrast, less information is available from the Neogene record and particularly from  
23 localities at low latitudes, with an additional and considerable bias in favor of craniodental  
24 rather than postcranial remains. In this contribution, we provide comparative descriptions of  
25 several postcranial bony elements ascribed to *Simomyiodon uccasamamensis*, a moderate-  
26 sized extinct mylodontine from the Andean Altiplano. This species was particularly abundant  
27 during latest Miocene–late Pliocene times in the high altitudes of the Andean Cordillera, and  
28 so far represents the best known mylodontine from the Neogene of South America. Its  
29 anatomy is compared with that of several extinct terrestrial sloths, with the aim of using the  
30 observed morphologies to elucidate taxonomy, phylogeny, and locomotion. From a  
31 morphofunctional perspective, the postcranium of *S. uccasamamensis* is consistent with that  
32 of a terrestrial graviportal quadruped, with moderate climbing and digging capabilities.  
33  
34  
35  
36  
37  
38  
39  
40  
41  
42  
43  
44  
45  
46  
47  
48  
49  
50  
51  
52

53 **Key words:** anatomy, extinct sloth, evolution, Mylodontinae, postcranium, skeleton,  
54  
55  
56  
57  
58  
59  
60



1  
2  
3 EXTANT SLOTHS (Folivora) are only represented by two genera, *Bradypus* and  
4  
5 *Choloepus*, restricted to tropical American rainforests, whereas their extinct taxonomic  
6  
7 richness was conspicuously greater (e.g., McKenna & Bell 1977; Gaudin 2004; Gaudin &  
8  
9 Croft 2015). This clade, together with anteaters (Vermilingua) and armadillos, pampatheres,  
10  
11 and glyptodonts (Cingulata), comprise Xenarthra, one of the four major lineages of placental  
12  
13 mammals (Meredith *et al.* 2011; O’Leary *et al.* 2013).  
14  
15

16  
17 Sloths comprise a significant component of late Cenozoic South American fossil  
18  
19 mammalian assemblages, with more than 90 recorded genera (McKenna & Bell 1997; Pujos  
20  
21 *et al.* 2017). Mylodontidae constitutes one of the major folivoran subdivisions, ranging  
22  
23 chronologically from the late Oligocene to the Pleistocene–Holocene interval, and  
24  
25 geographically to cover North and South America almost entirely (e.g., Pujos & De Iuliis  
26  
27 2007; McDonald & De Iuliis 2008; Shockey & Anaya 2011; Gaudin & Croft 2015; Boscaini  
28  
29 *et al.* 2019a). Morphology-based phylogenies did not seem to support relationships between  
30  
31 modern sloths and extinct mylodontids (e.g., Gaudin 2004; Varela *et al.* 2018). However,  
32  
33 recent molecular phylogenetic analyses suggest that the living two-toed sloth *Choloepus*  
34  
35 could be an extant member of Mylodontidae (Delsuc *et al.* 2019; Presslee *et al.* 2019).  
36  
37  
38  
39

40 Among Mylodontidae, Mylodontini and Lestodontini are sister clades that independently  
41  
42 radiated across South and North America between the late Miocene and the late Pleistocene  
43  
44 (Boscaini *et al.* 2019a). Both groups comprised moderately- to large-sized and even gigantic  
45  
46 quadrupedal herbivores, the majority of which exhibited grazing adaptations (Pujos *et al.*  
47  
48 2012). In general, Pleistocene Mylodontidae are well known, but less information is available  
49  
50 for Paleogene and Neogene members. This is especially true for Mylodontini, in which the  
51  
52 earlier and smaller representatives are far less well known than the larger and more recent  
53  
54 forms.  
55  
56  
57  
58  
59  
60

1  
2  
3 The Neogene Mylodontini species *Simomyodon uccasamamensis* is an endemic taxon  
4 from late Miocene–late Pliocene deposits of the Andean Altiplano (Saint-André *et al.* 2010;  
5 Boscaini *et al.* 2019b; Quiñones *et al.* 2019). This species was erected by Saint-André *et al.*  
6 (2010), and new abundant remains from the Bolivian Altiplano were subsequently studied by  
7 Boscaini *et al.* (2019b, c). In these works, many craniodental elements were considered,  
8 allowing for an assessment of both interspecific variation among Neogene mylodontines  
9 (Boscaini *et al.* 2019b) and the intraspecific variation within *S. uccasamamensis*, possibly  
10 related to sexual dimorphism (Boscaini *et al.* 2019c). Abundant fossils of this species were  
11 recovered in Neogene fossil-bearing Bolivian sites, from the departments of La Paz, Oruro  
12 and Potosí (Fig. 1; Boscaini *et al.* 2019b). More precisely, fossil remains come from the latest  
13 Miocene/early Pliocene of Choquecota, the early Pliocene of Casira, Inchasi and Pomata-  
14 Ayte, and the late Pliocene of Ayo Ayo-Viscachani (for further information on these  
15 localities, see Boscaini *et al.* 2019b). Recently, Quiñones *et al.* (2019) reported new remains  
16 of *S. uccasamamensis* from Casira, thereby extending the geographic range of this taxon to  
17 the Argentine side of the Casira Basin. Interestingly, the chronological distribution of *S.*  
18 *uccasamamensis* is bracketed between two major faunal turnover events which took place in  
19 the Bolivian highlands, i.e., the Miocene–Pliocene and the Pliocene–Pleistocene transitions  
20 (Hoffstetter 1986; Marshall *et al.* 1983; Marshall & Sempéré 1991).  
21  
22  
23  
24  
25  
26  
27  
28  
29  
30  
31  
32  
33  
34  
35  
36  
37  
38  
39  
40  
41  
42  
43  
44

45 In the Neogene fossil record of early South American mylodontines, postcranial elements  
46 are relatively rare. Indeed, the appendicular anatomy of the South American mylodontines  
47 *Glossotheridium chapadmalense* (southeastern Argentina, early Pliocene; Kraglievich 1925)  
48 and *Pleurolestodon acutidens* (Argentina, late Miocene; Rovereto 1914), is represented only  
49 by a single humerus and a single astragalus, respectively. A greater number of postcranial  
50 elements, including several autopodial elements, are known for the North American  
51  
52  
53  
54  
55  
56  
57  
58  
59  
60

1  
2  
3 *Paramylodon garbanii* (= '*Glossotherium*' *chapadmalense*; Mexico and USA, Pliocene;  
4  
5 Robertson 1976; Montellano-Ballesteros & Carranza-Castañeda 1986).  
6

7  
8 The new abundant material of *S. uccasamamensis* from Casira, Inchasi, Pomata-Ayte and  
9  
10 Ayo Ayo-Viscachani now allows for an almost complete characterization of the appendicular  
11  
12 anatomy of this extinct sloth, thereby making this taxon one of the best known Neogene  
13  
14 mylodontines from South America. We provide here a comprehensive analysis of the  
15  
16 postcranial anatomy of *S. uccasamamensis*, and particularly its appendicular elements. The  
17  
18 phylogenetic signal and functional implications of many features are also discussed. The  
19  
20 characterization of the postcranial anatomy of *S. uccasamamensis* is of great interest to  
21  
22 further our understanding of the evolutionary changes that occurred in Mylodontidae. It  
23  
24 provides new information for morphology-based phylogenetic analyses and paleobiological  
25  
26 reconstructions of extinct sloths.  
27  
28  
29  
30  
31

## 32 33 **MATERIAL AND METHODS**

### 34 35 36 37 *Fossil sample*

38  
39  
40  
41  
42 The new postcranial elements for *Simomylon uccasamamensis* described here were  
43  
44 recovered from several localities on the Bolivian Altiplano (Fig. 1; Boscaini *et al.* 2019b).  
45  
46 These fossils are deposited in the MNHN-Bol, MNHN, and UF collections (see abbreviations  
47  
48 below). The complete list of fossil materials and their provenance is reported in Supporting  
49  
50 Information, Appendix S1. These postcranial elements were compared with their homologues  
51  
52 in several mylodontid and non-mylodontid taxa (see Supporting Information, Appendix S2).  
53  
54 Whenever possible, comparisons were made by first-hand examination of the specimens, but  
55  
56 we sometimes relied on high-quality photographs or bibliographic sources. Recent studies on  
57  
58  
59  
60

1  
2  
3 appendicular anatomy of extinct sloths were consulted as sources of information for muscle  
4 attachments (see Toledo *et al.* 2013, 2015; Amson *et al.* 2015*a, b*; and references therein).  
5  
6

7       Regarding the axial postcranium, only a small portion of the pelvis and  
8  
9 isolated/fragmented vertebrae and ribs have been discovered, thereby impeding a reliable  
10 assessment of the axial morphology. For this reason, the comparative description is mainly  
11 centered around the elements of the forelimb and hind limb. For these bones, the presence of  
12 multiple specimens of the same element, in some cases, also allowed observations regarding  
13 their intraspecific variation (Boscaini *et al.* 2019*c*). Measurements for all specimens were  
14 taken with a digital caliper to the nearest 0.1 mm (Supporting Information, Appendix S3).  
15  
16  
17  
18  
19  
20  
21  
22  
23  
24  
25

## 26       *Abbreviations*

27  
28  
29

30       *Anatomical abbreviations.* mtc, metacarpal; mtt, metatarsal.  
31  
32  
33  
34

35       *Institutional abbreviations.* AMNH, American Museum of Natural History, New York,  
36 USA; AMU-CURS, Colección de Paleontología de Vertebrados de la Alcaldía de Urumaco,  
37 Urumaco, Venezuela; CIAAP, Centro de Investigaciones Antropológicas, Arqueológicas y  
38 Paleontológicas, Coro, Venezuela; F:AM, Frick collection, American Museum of Natural  
39 History, New York, USA; FMNH, Field Museum of Natural History, Chicago, USA; IVIC,  
40 Instituto Venezolano de Investigaciones Científicas, Caracas, Venezuela; JUY-P, Museo de  
41 Geología, Mineralogía y Paleontología, Instituto de Geología y Minería, Universidad  
42 Nacional de Jujuy, San Salvador de Jujuy, Argentina; MACN, Museo Argentino de Ciencias  
43 Naturales “Bernardino Rivadavia,” Buenos Aires, Argentina; MCN, Museo de Ciencias  
44 Naturales, Caracas, Venezuela; MLP, Museo de La Plata, La Plata, Argentina; MNHN,  
45 Muséum national d’Histoire naturelle, Paris, France; MNHN-Bol, Museo Nacional de  
46  
47  
48  
49  
50  
51  
52  
53  
54  
55  
56  
57  
58  
59  
60

1  
2  
3 Historia Natural de Bolivia, La Paz, Bolivia; ROM, Royal Ontario Museum, Toronto,  
4  
5 Canada; UCMP, Museum of Paleontology, University of California, Berkeley, USA; UF,  
6  
7 University of Florida, Florida Museum of Natural History (FLMNH), Gainesville, USA;  
8  
9 USNM, National Museum of Natural History, Smithsonian Institution, Washington, D.C.,  
10  
11 USA; YPM-PU, Princeton University collection housed at Peabody Museum, Yale  
12  
13 University, New Haven, USA.  
14  
15  
16  
17  
18

## 19 SYSTEMATIC PALAEOLOGY

20  
21  
22  
23  
24 XENARTHRA Cope, 1889

25  
26 PILOSA Flower, 1883

27  
28 FOLIVORA Delsuc *et al.*, 2001

29  
30 MYLODONTIDAE Gill, 1872

31  
32 MYLODONTINAE Gill, 1872

33  
34 *Simomyodon* Saint-André *et al.*, 2010

35  
36 *Simomyodon uccasamamensis* Saint-André *et al.*, 2010

37  
38 (Figs 2–14; Supporting Information, Appendices S1, S3)

### 39 40 41 42 *Synonyms*

43  
44 *Glossotheriscum dalenzae* Saint-André, 1994: 174–183, fig. 18, pl. 13.

45  
46 *Simotherium uccasamamense* Saint-André, 1994: 184–228, figs. 19–20, pls. 14–20.

47  
48 *Glossotheridium chapadmalense*: Anaya & MacFadden, 1995: 94–98, figs. 3–5, tab. 1, nec  
49  
50 Kraglievich 1925.

51  
52 *Pleurolestodon dalenzae* Saint-André *et al.* 2010: 261–269, figs. 2–4, tab. 1.

53  
54 Mylodontinae indet. Anaya & MacFadden, 1995: 98–99, figs 6–7.

55  
56 Mylodontidae gen. indet. sp. indet. Quiñones *et al.* 2019: 8, fig. 6, tab. 2.  
57  
58  
59  
60

1  
2  
3 Mylodontinae gen. indet. sp. indet. Quiñones *et al.* 2019: 8–9, fig. 7, tab. 2.  
4

5 *Simomyiodon* cf. *S. uccasamamensis* Quiñones *et al.* 2019: 10–13, figs 9–10, tab. 3.  
6  
7  
8  
9

10 *Referred material*  
11

12 See Supporting Information, Appendix S1  
13  
14  
15

16 *Measurements*  
17

18 See Supporting Information, Appendix S3  
19  
20  
21  
22  
23

24 *Revised postcranial diagnosis*  
25

26 [The following diagnosis of *S. uccasamamensis* is based on postcranial traits, and is  
27 intended to complement the craniodental diagnosis reported in Boscaini *et al.* (2019b: p.  
28 465)]. In *S. uccasamamensis*, the lateral margin of the supinator crest of the humerus exhibits  
29 a convex profile, and the lateral and medial humeral epicondyles are equally expanded in  
30 anterior view. The radius displays a marked convexity of its anterior margin in lateral view.  
31 In the manus, the mediolateral width of the trapezoid is greater than its dorsopalmar length,  
32 and the magnum can be either free or fused with the third metacarpal. The tibia is  
33 mediolaterally narrow in relation to total length (ratios ranging from 0.18 and 0.30),  
34 possessing two large grooves for the passage of tendons on the posteromedial margin of the  
35 distal epiphysis. In the pes, the calcaneum displays a well-developed sustentacular process.  
36 The astragalus exhibits a well-marked sulcus tali, a flat surface of the discoid process in  
37 lateral view, and a moderately obtuse discoid-odontoid angle (ranging between 90° and 115°)  
38 observable in either anterior or posterior views. The third metatarsal is dorsopalmarly thin in  
39 relation to its total length (ratios ranging from 0.23 and 0.31), and bears a distinct facet for  
40  
41  
42  
43  
44  
45  
46  
47  
48  
49  
50  
51  
52  
53  
54  
55  
56  
57  
58  
59  
60

1  
2  
3 the second metatarsal proximally. The fifth metatarsal has an arched ventral profile in lateral  
4  
5 view. Small, subspherical osteoderms are present.  
6  
7  
8  
9

## 10 RESULTS

### 11 12 13 14 *Comparative description*

15  
16  
17  
18  
19 *Scapula.* The anatomy of the scapula of *S. uccasamamensis* was previously unknown  
20  
21 (Saint-André *et al.* 2010). The available scapula, MNHN-Bol V 3718 (Fig. 2), is associated  
22  
23 with a skull (Boscaini *et al.* 2019b: fig. 8), and therefore its assignment to *S. uccasamamensis*  
24  
25 is clear. The scapular morphology of mylodontid sloths is very conservative, so that the main  
26  
27 differences are essentially size-related. The scapula of *Simomylodon* is very similar in shape  
28  
29 not only to the homologous element in *Glossotherium*, *Mylodon* and *Paramylodon*, but also  
30  
31 in the lestodontines (Owen 1842; Stock 1925; Webb 1989). Scapulae of *Catonyx* and  
32  
33 *Scelidotherium* appear slightly more elongated anteroposteriorly, due to the more acute angle  
34  
35 between the vertebral and posterior borders (McDonald 1987).  
36  
37  
38  
39

40 In lateral view, the scapula of *S. uccasamamensis* exhibits a strong scapular spine, which  
41  
42 divides the anterior supraspinous fossa from the posterior infraspinous fossa, and served as an  
43  
44 attachment area for a well-developed spinodeltoideus muscle, as well as part of the trapezius  
45  
46 complex. The supraspinous and infraspinous fossae are large and roughly equal in size; the  
47  
48 former housed the supraspinatus muscle and the latter the infraspinatus muscle. The  
49  
50 secondary spine is confined to the posterior border, delimiting a very reduced post-scapular  
51  
52 fossa (Fig. 2), which housed both the triceps brachii caput longus and teres major muscles.  
53  
54 The scapular spine extends ventrally into the acromion process, which extends anteriorly to  
55  
56 fuse with the coracoid process, forming the acromiocracoid arch typical of sloths (e.g.,  
57  
58  
59  
60

1  
2  
3 Engelmann 1985; Rose & Emry 1993; McDonald 2003). This arch bears the articulation for  
4 the clavicle, which appears elliptical in outline (Fig. 2B). In ventral view, the glenoid cavity  
5 is pyriform, with its anteriormost end narrower mediolaterally than its posterior end. All these  
6 features are invariably present in Mylodontidae (e.g., Stock 1925; McDonald 1987). In  
7 ventral view, the long axes of the glenoid fossa and the clavicular facet form an acute angle  
8 in *Simomyodon* (Fig. 2B), as they do in other mylodontines (e.g., *Glossotherium* MACN Pv  
9 14066 and *Paramyodon* FMNH P14723) and in scelidotheriines (e.g., *Catonyx* FMNH  
10 P14238 and *Scelidotherium* FMNH P14274). In contrast, this angle is roughly orthogonal in  
11 *Lestodon* (MACN Pv 14648). Unfortunately, due to lack of preservation, this feature has not  
12 been observed in *Thinobadistes* and *Bolivartherium*, so that it remains unclear whether the  
13 morphology in *Lestodon* is typical for lestodontines in general.

14  
15 In medial view, the scapula of *S. uccasamamensis* MNHN-Bol V 3718 shows a  
16 pronounced posterior ridge of the subscapular fossa, forming a wide and triangular area for  
17 the teres minor muscle (and probably also the triceps brachii caput longus and the teres  
18 major; Fig. 2C). This feature is common in all known Mylodontinae, whereas this fossa is  
19 reduced in size and more posteriorly oriented in Scelidotheriinae.

20  
21  
22 *Humerus*. Seventeen humeral fragments assigned to *S. uccasamamensis* are available for  
23 study (Supporting Information, Appendix S1). However, the only complete specimen is the  
24 right humerus MNHN-Bol V 13367, depicted in Figure 3. The humerus of *S.*  
25 *uccasamamensis* is robust, with its distal end broader mediolaterally than its proximal end in  
26 anterior view (Fig. 3). In proximal view (Fig. 3A), the humeral head is subspherical in shape,  
27 and adjacent anteromedially to the lesser tuberosity (where the subscapularis inserted) and  
28 anterolaterally to the greater tuberosity (where both the supra- and infraspinatus muscles  
29 inserted). The latter is more protruded externally than the former in proximal view (Fig. 3A),  
30  
31  
32  
33  
34  
35  
36  
37  
38  
39  
40  
41  
42  
43  
44  
45  
46  
47  
48  
49  
50  
51  
52  
53  
54  
55  
56  
57  
58  
59  
60



1  
2  
3 a widespread feature in Mylodontidae (Boscaini *et al.* 2019a: char. 304). An exception is  
4 represented by *Nematherium* (YPM-PU 15374 and FMNH P13131), in which the opposite  
5 condition is present. The latter conformation is also observed in *Hapalops* and *Bradypus*,  
6 thereby suggesting that this condition is primitive for sloths (Boscaini *et al.* 2019a: char.  
7 304).  
8  
9

10  
11  
12 The greater tuberosity continues ventrally into the deltopectoral shelf, which shows a  
13 rugose surface for attachment of the muscles in the pectoralis and deltoid complex (Fig. 3B).  
14  
15 The deltopectoral shelf faces anterolaterally and has an oblique distal margin, a  
16 plesiomorphic feature of Mylodontinae (Boscaini *et al.* 2019a: chars 301–302). In contrast, in  
17  
18 *Nematherium*, *Scelidotherium* and *Catonyx*, the deltopectoral crest shows a derived  
19 morphology. In these taxa, the deltopectoral crest has a more horizontal distal margin and  
20 faces more anteriorly, overlapping the ascending entepicondylar ridge in anterior view  
21  
22 (Boscaini *et al.* 2019a: chars 301–302).  
23  
24  
25  
26  
27  
28  
29  
30  
31  
32

33 In anterior view, the lateral epicondyle is expanded laterally, and delimited by a laterally  
34 convex supinator crest (Fig. 3B), where the brachioradialis, supinator and many extensor  
35 muscles of the manus attached. The supinator crest curves medially to reunite with the  
36 humeral shaft in close proximity to the end of the deltopectoral shelf, as observed in  
37  
38 *Thinobadistes*, *Pseudopreprotherium* and *Nematherium* (Boscaini *et al.* 2019a: char. 303). In  
39 the other Mylodontidae, the profile of the supinator crest is less regular and its most distal  
40 portion is proximodistally vertical. As is typical for mylodontids, the medial epicondyle,  
41 which served as an attachment site for many manual flexor muscles, bears a distinct proximal  
42 process (Boscaini *et al.* 2019a: char. 307). Furthermore, as in all Mylodontinae, the  
43 entepicondylar foramen is lacking (Fig. 3B; McDonald & De Iuliis 2008; Boscaini *et al.*  
44 2019a: char. 306). The medial and lateral epicondyles extend transversely to approximately  
45 the same degree (Fig. 3B), a condition that is also observed in *Thinobadistes* (Webb 1989)  
46  
47  
48  
49  
50  
51  
52  
53  
54  
55  
56  
57  
58  
59  
60

1  
2  
3 and *Pseudopreotherium* (Hirschfeld 1985). In *Nematherium*, *Catonyx* and *Scelidotherium*,  
4 the medial epicondyle is wider than the lateral epicondyle, whereas the opposite is true in the  
5 remainder of the Mylodontinae (Boscaini *et al.* 2019a: char. 308).  
6  
7

8  
9  
10 In distal view (Fig. 3C), both epicondyles are directed posteriorly, as is also observed in  
11 *G. robustum*, *P. harlani*, *M. darwinii* and *G. chapadmalensis*. In *Pseudopreotherium*, the  
12 medial epicondyle is directed medially, whereas in *Lestodon* it is directed anteriorly. In  
13 *Thinobadistes*, the humerus varies in this feature: both epicondyles are either directed  
14 posteriorly or mediolaterally in distal view (Boscaini *et al.* 2019a: chars 311–312). In the  
15 same view, the capitulum and the trochlea of *Simomyodon* have approximately the same  
16 anteroposterior depth (Fig. 3C), a widespread feature among mylodontids, with the exception  
17 of *Scelidotherium* and *Catonyx*, in which the trochlea is consistently deeper anteroposteriorly  
18 than the capitulum. However, the trochlea of *S. uccasamamensis* appears transversely wider  
19 than the capitulum (Fig. 3C), in this way more closely resembling *G. chapadmalensis* and *P.*  
20 *harlani*, rather than *M. darwinii* and *G. robustum* among Mylodontini. In the latter taxa, the  
21 mediolateral widths of the capitulum and trochlea are equivalent (Boscaini *et al.* 2019a: chars  
22 309–310).  
23  
24  
25  
26  
27  
28  
29  
30  
31  
32  
33  
34  
35  
36  
37  
38  
39  
40  
41

42 *Radius*. Features on the radius of *S. uccasamamensis* can be observed in eight specimens,  
43 two of which are complete: MNHN.F.AYO180 (Saint-André *et al.* 2010: fig. 11) and  
44 MNHN-Bol V 3375 (Fig. 4). The general morphology of the radius of *S. uccasamamensis* is  
45 more similar to that of *Pseudopreotherium* (Hirschfeld 1985) and the lestodontines (Webb  
46 1989), rather than the remaining Mylodontinae. In fact, the ratio between the anteroposterior  
47 radial depth, measured at midshaft, and the proximodistal length reaches its maximum values  
48 among mylodontids in the genera *Pseudopreotherium*, *Thinobadistes*, *Lestodon* and  
49 *Simomyodon* (Boscaini *et al.* 2019a: char. 314). This is due to the presence of a well-  
50  
51  
52  
53  
54  
55  
56  
57  
58  
59  
60

1  
2  
3 developed pronator ridge (for attachment of the pronator teres muscle) that makes the anterior  
4 border of the radius anteriorly convex in lateral view (Fig. 4B). In contrast, the posterior  
5 border is straight in lateral view (Fig. 4B). This combination of features is observed in  
6  
7  
8  
9  
10 *Simomyodon*, *Pseudopreotherium*, *Thinobadistes* and *Lestodon* (Hirschfeld 1985; Webb  
11 1989). In other Pleistocene Mylodontinae, like *Mylodon*, *Glossotherium* and *Paramylodon*,  
12 the radius has a more straight and stocky structure, lacking a well-developed pronator crest  
13 (Owen 1842; Stock 1925; McAfee 2016; Cartelle *et al.* 2019). In contrast, *Nematherium*,  
14  
15  
16  
17  
18  
19  
20  
21  
22  
23  
24  
25  
26  
27  
28  
29  
30  
31  
32  
33  
34  
35  
36  
37  
38  
39  
40  
41  
42  
43  
44  
45  
46  
47  
48  
49  
50  
51  
52  
53  
54  
55  
56  
57  
58  
59  
60

This latter morphology results in a bend of the shaft that is typical of scelidotheriines (McDonald 1987; Boscaini *et al.* 2019a: chars 316–317). The radial or bicipital tuberosity of *Simomyodon* is conspicuous, proximodistally elongated, and marked by a slightly concave terminal surface (Fig. 4C–D).

In *Simomyodon*, the shape of the radial head is piriform, with straight lateral and medial sides, as in the majority of Mylodontidae. In contrast, the radial head is generally more rounded in *Nematherium*, *Scelidotherium*, *Catonyx*, *Thinobadistes* (Boscaini *et al.* 2019a: char. 315) and *G. wegneri* (De Iuliis *et al.* in press). However, the proportions of the distal articulation of the radius do not vary conspicuously among mylodontids (Boscaini *et al.* 2019a: char. 320). The distal radius is marked by a low ridge separating the facets for the scaphoid and the lunar in MNHN.F.AYO180 (Saint-André *et al.* 2010), but this ridge is absent in MNHN-Bol V 3375 (Fig. 4F). The former condition is widespread in Mylodontidae (e.g., Rautenberg 1906; Haro *et al.* 2017), whereas the latter condition is typical of *Pseudopreotherium* and the scelidotheriines (Hirschfeld 1985; McDonald 1987). A similar intraspecific variation of the latter feature has also been observed in *G. robustum* (Rautenberg 1906; Pitana 2011).

1  
2  
3  
4  
5  
6 *Ulna*. An almost complete ulna, lacking part of the olecranon and the distal epiphysis, is  
7  
8 available for description: MNHN-Bol V 3717 (Fig. 5; Supporting Information, Appendix S1).  
9  
10 The ulna was previously unknown for *S. uccasamamensis* (Saint-André *et al.* 2010) and its  
11  
12 recovery in association with a complete cranium (Boscaini *et al.* 2019b: fig. 7) allows a  
13  
14 definitive assignment to this species. The ulna is relatively short proximodistally and deep  
15  
16 anteroposteriorly, as in other Mylodontinae, with the exception of *Pseudopreotherium*  
17  
18 (Hirschfeld 1985). In the latter taxon, but also in *Nematherium*, *Scelidothorium* and *Catonyx*,  
19  
20 the ulna is narrower anteroposteriorly and more elongated proximodistally (Boscaini *et al.*  
21  
22 2019a: char. 322). The olecranon meets the posterior edge of the ulna at a wide angle,  
23  
24 comparable to the condition in all Mylodontinae with the exception of *Thinobadistes segnis*  
25  
26 (Webb 1989) and *Glossotherium wegneri* (De Iuliis *et al.* in press). In these latter taxa, the  
27  
28 proximal and posterior borders of the ulna meet at an almost orthogonal angle (Webb 1989;  
29  
30 De Iuliis *et al.* in press), a feature also observed in *Scelidothorium* and *Catonyx* (McDonald  
31  
32 1987; Boscaini *et al.* 2019a: char 323).

33  
34  
35  
36  
37 In anterior view, the trochlear notch of *Simomyodon* is marked by well-defined lateral  
38  
39 and medial facets, which both culminate at the same height at the level of the anconeal  
40  
41 process (Fig. 4A), as in *Paramyodon harlani* and *P. garbanii*. The lateral portion is more  
42  
43 proximally extended than the medial portion in *G. robustum*, *M. darwinii* and *L. armatus*,  
44  
45 whereas the opposite condition is observed in *Thinobadistes*, *Nematherium*, *Catonyx* and  
46  
47 *Scelidothorium*. The radial notch is also well defined, and its area is relatively wider in  
48  
49 *Simomyodon* (in comparison with the trochlear notch) than in *Mylodon*, *Glossotherium* and  
50  
51 *Paramyodon* (Boscaini *et al.* 2019a: chars 324–325).  
52  
53  
54

55  
56 In posterior view (Fig. 5C), the width of the ulna decreases from proximal to distal, as  
57  
58 observed in all Mylodontinae with the exception of *Pseudopreotherium*. In the latter, but  
59  
60

1  
2  
3 also in *Nematherium*, *Scelidotherium* and *Catonyx*, the ulna is columnar in posterior view,  
4 with a uniform transverse width along its entire length (Boscaini *et al.* 2019a: char. 326).  
5  
6 These four latter genera also differ from other mylodontids in the inclination of the distal  
7 articular facet for the cuneiform. In these taxa, the long axis of the facet is oblique, so that in  
8 lateral view its anterior margin is more proximal than its posterior edge (McDonald 1987).  
9  
10 However, in all the other Mylodontidae, the distal articular facet is at a right angle to the long  
11 axis of the shaft in lateral view (Boscaini *et al.* 2019a: char. 328). Unfortunately, this latter  
12 feature cannot be observed in *S. uccasamamensis* because the distal ulnar epiphysis is  
13 missing (Fig. 5).  
14  
15  
16  
17  
18  
19  
20  
21  
22  
23  
24  
25

26 *Manus*. The manus of *S. uccasamamensis* has the typical mylodontid conformation, with  
27 five metacarpals and ungual phalanges on the first three digits only. This pattern is present in  
28 the manus of almost all known mylodontid sloths, with the exception of *Scelidotherium*, in  
29 which the ungual is also missing on the first digit (McDonald 1987).  
30  
31  
32  
33  
34

35 Several elements of the manus of *S. uccasamamensis* are available and preserved three-  
36 dimensionally (Figs 6–8), allowing an extensive characterization of its morphology. Two of  
37 these elements, the scaphoid and trapezium, were described by Saint-André *et al.* (2010), and  
38 subsequently glued into an assembled manus, rendering it impossible to observe all of their  
39 features in detail. For this reason, photos of these two elements (Fig. 6) were taken directly  
40 from Saint-André *et al.* (2010).  
41  
42  
43  
44  
45  
46  
47  
48

49 The scaphoid of *Simomylodon* (Fig. 6A–B) is similar in shape to that of other  
50 mylodontids. It bears an elongated medial process that supports the facet for the co-ossified  
51 trapezium and first metacarpal (carpal-metacarpal complex). The latter facet is separated  
52 from the facet for the trapezoid as in all Mylodontinae, and in contrast with Scelidotheriinae,  
53 in which the two facets are contiguous (McDonald 1987). In *Nematherium*, *Scelidotherium*  
54  
55  
56  
57  
58  
59  
60

1  
2  
3 and *Catonyx*, the medial process is relatively less elongated, and the scaphoid generally  
4 shows a blockier aspect than in other Mylodontidae. Accordingly, the former three genera  
5 exhibit a higher ratio between the minimum and maximum diameters (i.e., mediolateral width  
6 and proximodistal length) of the scaphoid (Boscaini *et al.* 2019a: char. 331). The facets for  
7 the trapezoid and magnum are separate and almost equal in size in MNHN.F.AYO180, the  
8 only available scaphoid of *S. uccasamamensis* (Fig. 6A–B; Saint-André *et al.* 2010).  
9  
10 However, in larger samples from other mylodontines, such as *Thinobadistes* and  
11  
12 *Paramylodon* (AMNH, FMNH, UF collections; Stock 1925), the arrangement of these facets  
13  
14 is highly variable.

15  
16  
17 The morphology of the lunar is extremely conservative in Mylodontidae (McDonald  
18  
19 1987). In the mylodontid lunars observed in the present study (see Supporting Information,  
20  
21 Appendices S1, S2), no reliable difference in proportions has been detected. The lunar-  
22  
23 scaphoid contact is separated into two distinct facets in MNHN.F.AYO111 (Fig. 6C), with  
24  
25 the proximal one clearly larger than the distal one. In MNHN.F.AYO180, the distal facet is  
26  
27 absent (Saint-André *et al.* 2010). The shape of the facets of the lunar-scaphoid contact, and  
28  
29 their mutual interconnection, are also variable in *Paramylodon*, *Thinobadistes* and several  
30  
31 scelidotheriines (McDonald 1987). On the proximal aspect of the lunar, the facet for the  
32  
33 radius is rounded and forms a wide convex surface (Fig. 6D), whereas on the distal aspect,  
34  
35 three contiguous facets can be differentiated (Fig. 6E). The latter are for connection with the  
36  
37 magnum medially, unciform centrally, and cuneiform laterally (Fig. 6E).  
38  
39

40  
41  
42 The general shape of the mylodontid cuneiform is that of a cube with a flat proximal facet  
43  
44 for the ulna, a more complex distal facet for the unciform, and smaller facets for the lunar and  
45  
46 pisiform (McDonald 1987). However, the cuneiform differs significantly in some proportions  
47  
48 among Mylodontidae (Haro *et al.* 2016; Boscaini *et al.* 2019a: chars 333–335). In  
49  
50 *Simomylodon* (Fig. 6F–H), together with all other mylodontines, the ratio of its dorsopalmar  
51  
52  
53  
54  
55  
56  
57  
58  
59  
60

1  
2  
3 depth and mediolateral width is quite uniform. This ratio is intermediate between those  
4  
5 registered for *Nematherium* (which shows the lowest, and hence a more mediolaterally  
6  
7 elongated cuneiform) and *Catonyx*, *Scelidotherium* and *Thinobadistes* (which show the  
8  
9 highest, and hence a more dorsopalmarly elongated cuneiform). The ratio between the  
10  
11 proximodistal length and mediolateral width of the cuneiform only differentiates  
12  
13  
14 *Nematherium* from the rest of the mylodontids. However, the ratio between the proximodistal  
15  
16 and dorsopalmar widths differentiates between Mylodontinae and Scelidotheriinae, with the  
17  
18 former having the higher ratios (cuneiform longer than deep). In the latter feature,  
19  
20  
21 *Thinobadistes* and *Paramylodon* show a certain degree of variation (Boscaini *et al.* 2019a:  
22  
23 chars 333–335). In the cuneiform of scelidotheriines, the lunar facet is positioned on a  
24  
25 process (McDonald 1987), which results in marked separation between the cuneiform and the  
26  
27 lunar. In contrast, this process is absent in Mylodontinae, so that the facet is adjacent to the  
28  
29 medial surface of the cuneiform (Boscaini *et al.* 2019a: char. 332). The latter configuration is  
30  
31 also observed in *Simomylodon* (Fig. 6G–H).

32  
33  
34  
35 The trapezoid of *S. uccasamamensis* (Fig. 6I–K) contacts the scaphoid, magnum and  
36  
37 mtc2, as in all mylodontid sloths. For this reason, the arrangement of the facets is similar in  
38  
39 all taxa considered in the present study. However, in *S. uccasamamensis* the mediolateral  
40  
41 width of the trapezoid is greater than its dorsopalmar length, a feature already noted by Saint-  
42  
43 André *et al.* (2010) and previously observed only in *P. garbanii* (Montellano-Ballesteros &  
44  
45 Carranza-Castañeda 1986). The opposite condition is found in other Mylodontidae, including  
46  
47 *S. leptcephalum*, *T. segnis*, *G. robustum*, *P. harlani* and *M. darwinii* (Supporting  
48  
49 Information, Appendix S2).

50  
51  
52  
53 No isolated magnum is so far known for *S. uccasamamensis*. The magnum is fused with  
54  
55 mtc3 in two of five specimens. This fusion is present in MNHN.F.AYO179 (Fig. 7I–M) and  
56  
57 MNHN.F.AYO180, whereas it is absent in the three isolated mtc3s: MNHN.F.VIZ27 (Fig.  
58  
59  
60

1  
2  
3 7F–H), MNHN.F.VIZ5 and MNHN-Bol V 12927. The fused specimens do not belong to the  
4  
5 same individual (both of them are left hand elements) and do not exhibit bone regrowth on  
6  
7 either side of the fused elements. This suggests that this connection is not related with any  
8  
9 pathology, but represents instead a peculiar trait of *Simomylodon*, that sometimes occurs in  
10  
11 the available sample. This condition is unknown in any other mylodontid. Even if the two  
12  
13 elements are fused, a transverse nutritive foramen is present at the level of their connection,  
14  
15 thereby allowing visual identification of the plane of separation (Fig. 7K, M). In this way, it  
16  
17 is possible to observe that the magnum has no visible connection with mtc2 in dorsal view.  
18  
19 The connection between the magnum and mtc2 is confined to a single facet on the palmar  
20  
21 edge, a typical feature of Mylodontinae (McDonald 1987). On the contrary, an extensive  
22  
23 contact between these two elements is visible on the dorsal side of the manus in  
24  
25 scelidotheriine sloths (Haro *et al.* 2016; Boscaini *et al.* 2019a: char. 339).  
26  
27  
28  
29

30  
31 In proximal view, the unciform of *S. uccasamamensis* displays a strong process for the  
32  
33 lunar, and a relatively short lateral platform for the cuneiform (Fig. 6L). The proximodistal  
34  
35 width of that bone exceeds its transverse width, a condition also observed in *M. darwinii*, *G.*  
36  
37 *robustum*, *P. harlani* and some specimens of *T. segnis*. The opposite pattern is observed in all  
38  
39 the other mylodontids (Boscaini *et al.* 2019a: char. 336). In distal view, the unciform displays  
40  
41 well-developed facets for metacarpals three, four and five (Fig. 6N). The former is located  
42  
43 medially and divided into two articular surfaces. Immediately lateral to these two facets is the  
44  
45 facet for mtc4, which is undivided, and abuts an even further laterally positioned and well-  
46  
47 developed facet for mtc5 (Fig. 6N). The extensive unciform/mtc5 contact is common in  
48  
49 Mylodontinae. However, a significant reduction of the unciform-fifth metacarpal facet is  
50  
51 observed in *Catonyx*, and the contact is completely absent in *Scelidotherium*, where mtc5  
52  
53 articulates only with mtc4 (McDonald 1987; Boscaini *et al.* 2019a: char. 342).  
54  
55  
56  
57  
58  
59  
60



1  
2  
3 A pisiform (Fig. 6O–P) and two manual sesamoids (Fig. 6Q–T) of *S. uccasamamensis*  
4 were also recovered. The pisiform shows a globose shape and a rugose external surface (Fig.  
5 6O–P), resembling that of *G. robustum*, *P. garbanii*, *P. harlani* and *T. segnis* (Owen 1842;  
6 6O–P), resembling that of *G. robustum*, *P. garbanii*, *P. harlani* and *T. segnis* (Owen 1842;  
7 Stock 1925; Robertson 1976; Webb 1989), whereas the element is more dorsopalmarly  
8 flattened in *M. darwinii* (Haro *et al.* 2016). The pisiform bears a single, flat and ovoid facet  
9 for the cuneiform (Fig. 6P).

10  
11  
12 Two distal sesamoids of mtc4 of *S. uccasamamensis* were also identified on the basis of  
13 their resemblance to their homologues in *M. darwinii* and *P. harlani* (Stock 1925; Haro *et al.*  
14 2016). The medial mtc4 distal sesamoid (Fig. 6Q–R) is consistently larger in size than the  
15 lateral one (Fig. 6 S–T). The sesamoids appear as tiny, proximodistally elongated bony  
16 elements, with a rugose external surface and a single concave facet for mtc4 (Fig. 6Q–T).

17  
18  
19 The trapezium and mtc1 are fused in *S. uccasamamensis* (Fig. 7A–B), forming the carpal-  
20 metacarpal complex, a feature observed in most sloths (McDonald 1977; Amson *et al.* 2015;  
21 Boscaini *et al.* 2019a: char 337). The two elements are separate in *Octodontotherium grande*  
22 (MNHN.F.DES231), and in some specimens of *Paramylodon harlani* (Stock 1925). The  
23 carpal-metacarpal complex possesses two separate proximal facets: a larger one for  
24 articulation with the scaphoid and a smaller, lateral one for articulation with mtc2. As in the  
25 majority of Mylodontinae, there is no facet for the trapezoid on the carpal-metacarpal  
26 complex (McDonald 1987), but a small contact has been reported for *M. darwinii* (Haro *et al.*  
27 2016). Distally, the carpal-metacarpal complex of *S. uccasamamensis* has a subspherical  
28 facet for the proximal phalanx of the first digit (Fig. 7A–B).

29  
30  
31 The second metacarpal of *S. uccasamamensis* (Fig. 7C–E) is relatively elongated and  
32 narrow mediolaterally. In proximal view, mtc2 bears a large articular surface for the  
33 trapezoid and a smaller one for the magnum. The latter, as noted above, is confined to the  
34  
35  
36  
37  
38  
39  
40  
41  
42  
43  
44  
45  
46  
47  
48  
49  
50

1  
2  
3 palmar side of the bone (Fig. 7C–E). The facet for the carpal-metacarpal complex on the  
4 lateral side is reduced, whereas the facet for mtc3 is wide and medially concave (Fig. 7C–D).  
5  
6

7  
8 As described above, mtc3 of *S. uccasamamensis* can be found either isolated (Fig. 7F–H)  
9 or fused with the magnum (Fig. 7I–M). In the isolated condition, mtc3 appears relatively long  
10 proximodistally and thin mediolaterally, especially near the midshaft, resembling that of *O.*  
11 *grande*, *Ps. confusum*, *Pa. garbanii*, *M. darwinii* and *M. ibseni* in this respect, whereas in the  
12 other mylodontids, this element is relatively shorter and thicker (Cartelle 1980; Boscaini *et*  
13 *al.* 2019a: char. 341). The articular surface for mtc2 is convex (Fig. 7), and the shafts of the  
14 two metacarpals (mtc2 and mtc3) are separated by a moderately developed proximomedial  
15 process on mtc3. This feature in *S. uccasamamensis* is similar to the condition observed in  
16 lestodontines. It is intermediate between the morphology of *Nematherium*, *Catonyx*,  
17 *Scelidotherium*, *Pseudopreotherium* and *Octodontotherium* (in which the process is shorter  
18 and the two metacarpals are closer together) and that of *Mylodon*, *Paramylodon* and  
19 *Glossotherium* (in which mtc2 and mtc3 show an even greater separation due to the presence  
20 of a longer process; Boscaini *et al.* 2019a: char. 340).  
21  
22  
23  
24  
25  
26  
27  
28  
29  
30  
31  
32  
33  
34  
35  
36

37  
38 Only a proximal fragment of mtc4 of *S. uccasamamensis* is available (Fig. 7N–P). In  
39 proximal view, the contacts with mtc3 and the unciform are contiguous, with the latter more  
40 extended dorsopalmarly than the former (Fig. 7N). On the lateral side, the facet for mtc5 is  
41 flat and triangular in outline (Fig. 7P).  
42  
43  
44  
45  
46

47  
48 The fifth metacarpal of *S. uccasamamensis* (Fig. 7Q–S) is similar in shape to that of other  
49 Mylodontinae such as *Thinobadistes*, *Paramylodon*, *Mylodon* and *Glossotherium* (Owen  
50 1842; Stock 1925; Webb 1989; Haro *et al.* 2016; McAfee 2016; Cartelle *et al.* 2019). This  
51 element is more gracile in scelidotheriines (McDonald 1987), and shorter and wider in  
52 *Lestodon* (MACN Pv 10760). In *Simomyodon*, the proximal portion of mtc5 shows two large  
53 adjacent facets for mtc4 and the unciform, respectively (Fig. 7Q–R). This conformation is  
54  
55  
56  
57  
58  
59  
60

1  
2  
3 observed in virtually all mylodontids with the exception of *Scelidotherium*, in which mtc5  
4 only contacts mtc4 proximally (McDonald 1987). In *Simomyodon*, there is no evidence for  
5 an articulation with the cuneiform, as also observed in *Catonyx* (McDonald 1987), *Lestodon*  
6 (MACN Pv 10760) and *Thinobadistes* (Webb 1989). However, in *Thinobadistes*, an  
7 extremely reduced surface articulation is visible in some specimens (e.g., AMNH F:AM  
8 102850). A small articulation between the cuneiform and mtc5 is present in *M. darwinii*  
9 (Haro *et al.* 2016), *P. harlani* (Stock 1925), *P. garbanii* (Montellano-Ballesteros & Carranza-  
10 Castañeda 1986), *G. robustum* (Owen 1842) and *G. phoenesis* (Cartelle *et al.* 2019). As in all  
11 mylodontids, the distal end of mtc5 bears a small ovoid facet for the proximal (and probably  
12 only) phalanx. This latter element, usually rudimentary, is not currently available for  
13 *Simomyodon*.

14  
15  
16  
17  
18  
19  
20  
21  
22  
23  
24  
25  
26  
27  
28  
29  
30  
31  
32  
33  
34  
35  
36  
37  
38  
39  
40  
41  
42  
43  
44  
45  
46  
47  
48  
49  
50  
51  
52  
53  
54  
55  
56  
57  
58  
59  
60  
The proximal and intermediate phalanges of MNHN-Bol V 3313 (Fig. 8A–G) are very  
similar in shape to those of *G. robustum* and *P. harlani* (Owen 1842; Stock 1925), and thus  
likely belonged to the right third digit of *S. uccasamamensis*. Also, the three ungual  
phalanges of MNHN.F.AYO180 (Fig. 8H–P) are likely those of the first three digits of the  
left hand, based on their relative size. The ungual phalanges are covered proximally by bony  
sheaths, which show different stages of completeness, and are pierced by paired subungual  
foramina on their ventral surface (Fig. 8H–P). The osseous ungual cores are almost circular  
in cross-section, as in *G. robustum* and *P. harlani* (Owen 1842; Stock 1925). As in *P. harlani*  
(Stock 1925), two symmetrical concavities mark the ventral side of the core, and are deeper  
in the ungual phalanx of the second digit (Fig. 8K–M) than the third digit (Fig. 8N–P). As  
already noted, the presence of three clawed digits on the manus is a widespread mylodontid  
feature, although not present in *Scelidotherium*, which lacks an ungual on digit 1 (Winge  
1915; McDonald 1987; Boscaini *et al.* 2019a: char. 343).

1  
2  
3 *Femur*. Twenty femora/femoral fragments of *S. uccasamamensis* have been recovered,  
4  
5 but only eight of them are relatively complete (Supporting Information, Appendix S1). Of  
6  
7 these eight, five appear larger and more robust than the other three, an indication of size-  
8  
9 based sexual dimorphism as suggested by Boscaini *et al.* (2019c). However, the following  
10  
11 descriptions and comparisons are valid for all the available femoral specimens.  
12  
13

14  
15 The femur of *S. uccasamamensis* (Fig. 9) is similar in shape to that of the other  
16  
17 Mylodontinae. The ratio between the mediolateral width at midshaft and proximodistal length  
18  
19 is similar among mylodontines, but is consistently higher in the scelidotheriines (McDonald  
20  
21 1987; Boscaini *et al.* 2019a: char. 344). As in all mylodontines, the femur of *Simomylodon* is  
22  
23 narrower distally than proximally in anterior view. In *Simomylodon*, the ratio between  
24  
25 maximum femoral condylar width and femoral length is similar to that of most other  
26  
27 Mylodontinae. This ratio is intermediate between the lowest value recorded for mylodontids,  
28  
29 that of *Pseudopreoptherium*, *Urumacotherium* and *Mirandabradys*, and the highest value  
30  
31 recorded, that of the scelidotheriines (Boscaini *et al.* 2019a: char. 345). Also, the ratio  
32  
33 between the intertrochanteric width and the proximodistal length of the femur is consistent  
34  
35 among mylodontids, with the scelidotheriines representing an exception, exhibiting the  
36  
37 highest observed values (Boscaini *et al.* 2019a: char. 347). Similarly, the ratio between the  
38  
39 anteroposterior depth and the mediolateral width measured at the femoral midshaft is similar  
40  
41 in all mylodontids, with *Catonyx* and *Scelidotherium* showing the lowest values (Boscaini *et*  
42  
43 *al.* 2019a: char. 348).  
44  
45  
46  
47  
48

49 In *Simomylodon*, the greater trochanter is broad mediolaterally and deep  
50  
51 anteroposteriorly, but is not elongated proximodistally (Fig. 9). In fact, it does not reach the  
52  
53 proximal level of the femoral head in anterior view, a feature shared with many mylodontids.  
54  
55 Basal megatherioid sloths like *Hapalops* are characterized by a nearly equivalent proximal  
56  
57 extension of the femoral head and the greater trochanter, but this morphology is only  
58  
59  
60

1  
2  
3 observed among mylodontids in *Pseudopreotherium* (Boscaini *et al.* 2019a: char. 350). The  
4  
5 greater trochanter of *S. uccasamamensis* shows a rugose area for attachment of gluteal  
6  
7 (gluteus minimus and medius) and femoral abductor (pyriformis) muscles. A vertical crest on  
8  
9 the anterior surface of the proximal femur marks the separation of these entheses (i.e., muscle  
10  
11 attachments, *sensu* Mariotti *et al.* 2007) from the origins of a powerful vastus complex (knee  
12  
13 extensors).

14  
15  
16 The femoral neck is moderately extended proximomedially in *Simomyodon* (Fig. 9). In  
17  
18 anterior view, the neck gradually decreases in width from its base to its contact with the edge  
19  
20 of the femoral head. This same morphology is observed in *Lestodon*, *Mylodon*,  
21  
22 *Glossotherium* and *Paramylodon* (Boscaini *et al.* 2019a: chars 351–352). In contrast,  
23  
24 *Thinobadistes* shows a more distinct sulcus surrounding the articular surface of the femoral  
25  
26 head, whereas *Catonyx* and *Scelidotherium* lack a conspicuous femoral neck (McDonald  
27  
28 1987; Webb 1989).

29  
30  
31 In posterior view (Fig. 9D), *S. uccasamamensis* exhibits a well-developed  
32  
33 intertrochanteric fossa and lacks the intertrochanteric ridge connecting the trochanters.  
34  
35 Among Mylodontidae, a real intertrochanteric ridge connecting the trochanters is present  
36  
37 only in *Baraguatherium takumara* (Rincón *et al.* 2016), resembling in this regard the  
38  
39 Santacrucean megatherioid *Hapalops* (Boscaini *et al.* 2019a: char. 349).

40  
41  
42 The femur of *Simomyodon* possesses a third trochanter that is elongated proximodistally,  
43  
44 but is not as laterally prominent as that in *Baraguatherium* and *Pseudopreotherium*  
45  
46 (Boscaini *et al.* 2019a: char. 353). This results in a relatively straight, vertical lateral edge of  
47  
48 the femoral shaft, which is the most common condition in mylodontids, as represented for  
49  
50 instance by *Glossotherium* and *Paramylodon* (Fig. 9; Owen 1842; Stock 1925; Cartelle *et al.*  
51  
52 2019). As in most ground sloths, this area acted as an extended insertion entheses for the  
53  
54  
55  
56  
57  
58  
59  
60

1  
2  
3 powerful gluteus maximus muscle and the iliotibial tract (= tensor fasciae latae), both flexors  
4  
5 and abductors of the femur.  
6

7  
8 In distal view (Fig. 9F), the femur of *Simomylodon* does not present remarkable  
9  
10 differences from other Mylodontinae such as *Glossotherium*, *Lestodon*, *Paramylodon*,  
11  
12 *Pseudopreotherium* and *Thinobadistes* (Owen 1842; Stock 1925; Robertson 1976;  
13  
14 Hirschfeld 1985; Webb 1989; Cartelle *et al.* 2019; Vargas-Peixoto *et al.* 2019). In all these  
15  
16 taxa the larger medial tibial condyle and the smaller lateral tibial condyle are confluent with  
17  
18 the patellar groove (Fig. 9F). In *Simomylodon*, the transverse width of the distal articular  
19  
20 surface of the femur is greater, in relation to its anteroposterior depth, than that of  
21  
22 *Pseudopreotherium* and *Thinobadistes*, thus resembling the condition of Mylodontini such  
23  
24 as *Glossotherium* and *Paramylodon* (Owen 1842; Stock 1925; Cartelle *et al.* 2019).  
25  
26  
27  
28  
29

30  
31 *Tibia.* The tibia of *S. uccasamamensis* is known from 16 specimens, 10 of which are  
32  
33 relatively complete (Supporting Information, Appendix S1). As is the case with the femora,  
34  
35 the complete tibiae vary in their general aspect: three of them are larger and more robust than  
36  
37 the remaining ones (Boscaini *et al.* 2019c). However, the descriptions and comparisons of the  
38  
39 tibiae of *S. uccasamamensis* are applicable to the entire sample.  
40  
41

42  
43 The tibia of *S. uccasamamensis* (Fig. 10A–F) is similar, in its general aspect, to the  
44  
45 homologous element in *Mylodon*, *Glossotherium*, and *Paramylodon*, but it also shares several  
46  
47 features in common with *Lestodon* and *Thinobadistes* (e.g., Owen 1842; Stock 1925; Webb  
48  
49 1989; Cartelle *et al.* 2019; Vargas-Peixoto *et al.* 2019). In lateral and medial views (Fig. 10A,  
50  
51 C), the tibia of *S. uccasamamensis* is straight, a common mylodontid feature (Boscaini *et al.*  
52  
53 2019a: char. 355). However, the diaphysis is fairly uniform in anteroposterior depth, as in  
54  
55 *Mylodon*, *Glossotherium* and *Paramylodon* (Owen 1842; Stock 1925; Cartelle *et al.* 2019),  
56  
57 whereas the diaphysis decreases in anteroposterior depth from the proximal to the distal end  
58  
59  
60

1  
2  
3 in lestodontines (Webb 1989; Vargas-Peixoto *et al.* 2019). The latter morphology is also  
4  
5 observed in *Pseudopreotherium* (Hirschfeld 1985), *Octodontotherium* (FMNH P13517) and  
6  
7 in scelidotheriines (McDonald 1987).  
8  
9

10 The ratio between the anteroposterior depth of the proximal epiphysis and the total tibial  
11  
12 length is greater than 0.35 in *Simomyodon*, as in several mylodontids, with the exceptions of  
13  
14 *Pseudopreotherium*, *Octodontotherium*, *Mirandabradys* and *Urumacotherium*, in which the  
15  
16 ratio is lower (Boscaini *et al.* 2019a: char. 357). At the distal end, the ratio between  
17  
18 anteroposterior depth and the total tibial length is high in *Simomyodon*, *Myloodon*,  
19  
20 *Paramyloodon* and *Glossotherium* (greater than 0.74). Lower values (between 0.60 and 0.74)  
21  
22 are consistently observed in *Scelidotherium*, *Catonyx*, *Pseudopreotherium* and  
23  
24 *Octodontotherium*. The values for *Lestodon* and *Thinobadistes* fall between these ranges  
25  
26 (Boscaini *et al.* 2019a: char. 358). The ratio between the maximum mediolateral width of the  
27  
28 proximal epiphysis and the total tibial length is always less than 0.6 in *Simomyloodon*, as in  
29  
30 *Catonyx*, *Pseudopreotherium*, *Octodontotherium* and *Thinobadistes*, whereas it is higher  
31  
32 than 0.6 in *Myloodon*, *Glossotherium* and *Paramyloodon*. This feature is variable in *Lestodon*  
33  
34 and *Scelidotherium* (Boscaini *et al.* 2019a: char. 359).  
35  
36  
37  
38  
39

40 In proximal view (Fig. 10E), the medial and lateral tibial condyles of *Simomyloodon* are  
41  
42 markedly unequal in size, with the former much larger than the latter, a typical feature of  
43  
44 terrestrial sloths (Boscaini *et al.* 2019a: chars 360–361). Both tibial condyles are concave, but  
45  
46 the lateral is nearly flat. As in *Pseudopreotherium*, *Octodontotherium* and the  
47  
48 scelidotheriines, the tibia of *Simomyloodon* lacks any trace of a groove anterior to the lateral  
49  
50 condyle. In all other mylodontids a groove is present (Boscaini *et al.* 2019a: char. 362); it  
51  
52 faces laterally and probably accommodated the tendon of origin of the extensor digitorum  
53  
54 longus muscle (Evans & de Lahunta 2013). The tibial tuberosity is, as in most ground sloths,  
55  
56  
57  
58  
59  
60

1  
2  
3 wide, shallow and massive, thereby indicating a powerful and wide insertion tendon for both  
4  
5 the quadriceps femoris and tensor fasciae latae muscles.  
6

7  
8 The medial intercondylar eminence is not particularly evident in mylodontid sloths, but it  
9  
10 is moderately developed in *Octodontotherium*, *Pseudopreopotherium* and *Mirandabradys*,  
11  
12 resembling the basal megatherioid *Hapalops* in this regard (Boscaini *et al.* 2019a: char. 363).  
13

14  
15 In medial, posterior and distal views (Fig. 10C, D, F), two deep grooves for the tendons  
16  
17 of the ankle extensor and digital flexor muscles are present on the postero-medial aspects of  
18  
19 the distal tibia of *S. uccasamamensis*. These grooves are separated by a strong bony crest.  
20  
21 The presence of these two well-separated grooves is also observed in *Pseudopreopotherium*,  
22  
23 *Thinobadistes* and *Lestodon*. In *Octodontotherium*, the scelidotheriines, as well as in the  
24  
25 megalonychid and nothrotheriid sloths, three distinct grooves are present (Stock 1925;  
26  
27 McDonald 1987; Amson *et al.* 2015b). In nothrotheriids, these grooves accommodated (from  
28  
29 anterior to posterior), the tendons for the tibialis posterior, flexor digitorum longus and flexor  
30  
31 hallucis longus muscles, respectively (McDonald 1987; Amson *et al.* 2015b). In contrast, in  
32  
33 *Mylodon*, *Glossotherium* and *Paramylodon* this area bears a single groove, which probably  
34  
35 accommodated all three tendons. The condition of *Simomylodon*, *Pseudopreopotherium* and  
36  
37 the lestodontines therefore appears to be intermediate between the other two configurations  
38  
39 (Boscaini *et al.* 2019a: char. 365). Given that the posterior groove is larger than the anterior  
40  
41 one in *Simomylodon* (Fig. 10C), the tendons for the flexor digitorum longus and flexor  
42  
43 hallucis longus muscles were probably housed together in this groove, whereas the tendon for  
44  
45 the tibialis posterior muscle likely occupied the anterior groove.  
46  
47  
48  
49

50  
51 In distal view (Fig. 10F), the facet for the astragalus dominates the articular surface of the  
52  
53 distal tibia. As in all sloths, it is composed of two concave surfaces, one subspherical for  
54  
55 articulation with the odontoid process of the astragalus and the other nearly flat for  
56  
57 articulation with the discoid process. The distal fibular facet is located in the posteromedial  
58  
59  
60



1  
2  
3 corner of the distal tibia, a position that is typical in Mylodontinae, with the exception of  
4  
5 *Pseudopreotherium* and *Octodontotherium*. In these two latter genera, as in the  
6  
7 scelidotheriines (McDonald 1987), the distal tibial facet for the fibula is longer  
8  
9  
10 anteroposteriorly (Boscaini *et al.* 2019a: char. 364).  
11  
12  
13

14  
15 *Patella, fibula and cyamella.* The patella is represented in *S. uccasamamensis* by two  
16  
17 specimens: MNHN-Bol V 3300 (Saint-André *et al.* 2010: fig. 17) and MNHN-Bol V 12518  
18  
19 (Fig. 10G–H). In anterior and posterior views, this bone is triangular in shape, and very  
20  
21 similar to that of *Glossotherium* and *Paramylodon* (Owen 1842; Stock 1925). However, the  
22  
23 patella of *Lestodon* and *Thinobadistes* is proximodistally longer, with a more pronounced  
24  
25 ventral process (Webb 1989). In posterior view, the articular surface with the femur is  
26  
27 transversely convex in the vicinity of its midpoint, but becomes medially and laterally  
28  
29 concave, as it does in all mylodontids. In *S. uccasamamensis*, these latter areas appear equal  
30  
31 in proximodistal extent in MNHN-Bol V 3300 (Saint-André *et al.* 2010: fig. 17), whereas  
32  
33 they are more asymmetrical in MNHN-Bol V 12518 (Fig. 10H), with the medial facet  
34  
35 elongated distally. Intraspecific variation in the shape of the patellar articular surface has  
36  
37  
38 been observed in specimens of *Lestodon* and *Thinobadistes* (Supporting Information,  
39  
40 Appendix S2).  
41  
42  
43

44  
45 Six fibulae of *S. uccasamamensis* (Fig. 10I–L) are available (Supporting Information,  
46  
47 Appendix S1). The fibula is conservative in its morphology among mylodontids (McDonald  
48  
49 1987). The ratio between the proximodistal length of the distal articular surface and the total  
50  
51 length of the fibula is, for example, similar in all mylodontids (Boscaini *et al.* 2019a: char.  
52  
53 366). This bone is mediolaterally narrow and anteroposteriorly broad as in all Mylodontinae,  
54  
55 in contrast to the condition in the scelidotheriines, in which it is more rounded in cross  
56  
57 section (McDonald 1987). Proximally and medially, the fibula carries a flat, anteroposteriorly  
58  
59  
60

1  
2  
3 elongate facet for the tibia and, more posteriorly, a smaller and more convex facet for the  
4  
5 cyamella.  
6

7  
8 In Mylodontidae, the presence of a cyamella (or fabella, or cyamo-fabella) has been  
9  
10 reported for *Scelidotherium* (Burmeister 1881) and *Myiodon* (Roth 1899). In other taxa, such  
11  
12 as *Catonyx*, *Scelidotherium*, *Paramylodon*, *Pseudopreotherium* and *Thinobadistes*, its  
13  
14 presence was inferred by the presence of articular surfaces on the proximal epiphyses of  
15  
16 either the tibia, the fibula or both (Stock 1925; Hirschfeld 1985; McDonald 1987; Webb  
17  
18 1989). In *S. uccasamamensis*, both right and left cyamellae are available in MNHN-Bol V  
19  
20 12518 (Fig. 10M–N, 11). The cyamella is roughly spherical and, on its medial side, bears  
21  
22 three contiguous but discrete facets (Fig. 10N). These are (from proximal to distal) for  
23  
24 articulations with the femur, tibia and fibula, respectively. The facet for the tibia is the largest  
25  
26 of the three (Fig. 10N). In proximal view, the femoral facet on the cyamella forms a  
27  
28 continuous articular surface with the lateral condyle of the tibia for the articulation with the  
29  
30 femur (Fig. 11C).  
31  
32  
33  
34  
35  
36  
37

38 *Pes.* Several tarsal and metatarsal bones of *S. uccasamamensis* are available for  
39  
40 description (Supporting Information, Appendix S1), but elements unequivocally attributable  
41  
42 to the pedal phalanges are so far lacking.  
43  
44

45 Only a single complete calcaneum of *S. uccasamamensis*, MNHN-Bol V 8541, has been  
46  
47 recovered (Fig. 12A–D). The posterior portion of the calcaneum corresponds to the tuber  
48  
49 calcis (entheses for gastrocnemius, soleus, and plantaris muscles), which contacted the  
50  
51 ground. This area is enlarged anteroposteriorly and mediolaterally, forming a triangular  
52  
53 surface that is typical of Mylodontinae (Fig. 12A–C). Only *Pseudopreotherium* exhibits a  
54  
55 tuber calcis in which the anteroposterior length is not markedly enlarged (Hirschfeld 1985;  
56  
57 Boscaini *et al.* 2019a: char. 374). However, the tuber calcis of *S. uccasamamensis* resembles  
58  
59  
60

1  
2  
3 that of *Pseudoprepotherium*, the lestodontines and the scelidotheriines, in lacking the strong  
4 mediolateral expansion observed on calcanei of *G. robustum* and *P. harlani* (Owen 1842;  
5 Stock 1925; Boscaini *et al.* 2019a: char. 373). As in all mylodontids, the tuber calcis of *S.*  
6 *uccasamamensis* is connected with the anterior articular portion by a neck region that is  
7 constricted dorsoventrally and mediolaterally (Fig. 12A–C). This neck in *S. uccasamamensis*  
8 is clearly shorter than that of scelidotheriines, which also lack a tendinous groove on the  
9 lateral and ventral sides (Fig. 12B–C). This groove probably housed the tendons of the  
10 peroneus longus and peroneus brevis muscles (McDonald 1987). Directly anterior to this  
11 groove, the articular portion of the calcaneum contacts the astragalus (Fig. 12E–H) and the  
12 cuboid (Fig. 13D–G). The calcaneal-astragal joint is divided into separate ectal and  
13 sustentacular facets, the former larger than the latter (Fig. 12D). In *S. uccasamamensis*, the  
14 sustentacular facet is located on a distinct medial process (Fig. 12A–D), the sustentaculum.  
15 The facet faces anteriorly and slightly laterally as in most ground sloths. The sustentaculum is  
16 not present in *Glossotherium* and *Paramylodon* (Owen 1842; Stock 1925; Boscaini *et al.*  
17 2019a: char. 375; Cartelle *et al.* 2019), where ectal and sustentacular facets are confluent, and  
18 no sulcus calcanei is evident. The ectal facet of *S. uccasamamensis* is anteroposteriorly  
19 elongated and saddle-shaped (anteroposteriorly convex and mediolaterally concave), whereas  
20 it is almost flat in *Glossotherium* and *Paramylodon* (Owen 1842; Stock 1925; Cartelle *et al.*  
21 2019). The cuboid facet is adjacent to the sustentacular facet, but separated by a ridge as in  
22 *Glossotherium* and *Paramylodon*, whereas in *Scelidotherium* these facets are separated by a  
23 smooth depression as in the basal megatherioid *Hapalops* (FMNH P13123).

24  
25  
26  
27  
28  
29  
30  
31  
32  
33  
34  
35  
36  
37  
38  
39  
40  
41  
42  
43  
44  
45  
46  
47  
48  
49  
50  
51  
52  
53  
54  
55  
56  
57  
58  
59  
60  
Nine astragali of *S. uccasamamensis* have been recovered (Supporting Information, Appendix S1). The general astragal proportions in *Simomylodon*, quantified by the ratio between the proximodistal and anteroposterior lengths (between 0.8 and 1.0), are similar to those of most Mylodontinae. The lowest values (< 0.8) are obtained in the basal

1  
2  
3 mylodontines *Octodontotherium* and *Pseudopreotherium*, and the highest values ( $> 1.0$ ) in  
4 the scelidotheriines *Catonyx* and *Scelidotherium* (Boscaini *et al.* 2019a: char. 367). In  
5  
6 *Simomylon*, the medial and lateral trochlear surfaces of the astragalus are modified, as in  
7  
8 all mylodontid sloths, to form a raised and globose odontoid process, and a flat, horizontal  
9  
10 and semicircular discoid facet (Fig. 12E, F, H). However, the angle formed by the odontoid  
11  
12 process and the discoid facet, observed in either anterior or posterior views, is quite different  
13  
14 among various mylodontids (Boscaini *et al.* 2019a: char. 368). The odontoid-discoid angle is  
15  
16 markedly obtuse ( $> 115^\circ$ ) in the scelidotheriines, as it is in the basal mylodontine *O. grande*  
17  
18 and the Pliocene North American species *P. garbanii*. It is moderately obtuse ( $> 90^\circ$  but  $<$   
19  
20  $115^\circ$ ) in most Mylodontinae, including *G. robustum*, *M. darwinii*, *Pa. harlani*, *Ps. confusum*,  
21  
22 *Pl. acutidens* and *S. uccasamamensis*. In contrast, this angle is orthogonal or acute ( $\leq 90^\circ$ ) in  
23  
24 the lestodontines. In the mylodontid astragalus, the discoid facet surrounds the odontoid  
25  
26 process both laterally and posteriorly. In lateral view, the facet has an anteroposterior  
27  
28 curvature in *Nematherium*, *Octodontotherium*, as well as in the scelidotheriines and the  
29  
30 lestodontines, whereas it is essentially flat in *Glossotherium*, *Mylodon*, *Paramylodon*,  
31  
32 *Pleurolestodon*, *Pseudopreotherium* and *Simomylon* (Fig. 12H; Boscaini *et al.* 2019a:  
33  
34 char. 369). As in all mylodontids, the astragalus of *S. uccasamamensis* exhibits a  
35  
36 proximodistally elongated facet for the fibula, located at the anteriormost limit of the discoid  
37  
38 facet, and visible in lateral view (Fig. 12H). The shape of this facet is quite variable  
39  
40 intraspecifically in *S. uccasamamensis*, as also observed in the large samples of *Paramylodon*  
41  
42 and *Thinobadistes*.

51  
52 As stated above, the ectal and sustentacular facets of the calcaneum are separated in *S.*  
53  
54 *uccasamamensis*. The same pattern is observed on the astragalus (Fig. 12G; Saint-André *et*  
55  
56 *al.* 2010), in which the two facets are separated by a deep sulcus tali. Both sulci delimit the  
57  
58 sinus tarsi, occupied by an interosseous ligament. The presence of a sulcus tali is considered  
59  
60

1  
2  
3 plesiomorphic among sloths (McDonald 1987). In *Glossotherium*, *Myiodon* and  
4  
5 *Paramyiodon*, these two facets coalesce into a uniform surface for the articulation with the  
6  
7 calcaneum (e.g., Gervais 1873; Kraglievich 1926; McDonald 1987; Webb 1989). The  
8  
9 plesiomorphic condition is found not only in *Simomyiodon*, but also in *Nematherium*,  
10  
11 *Octodontotherium*, *Pseudopreotherium*, *Pleurolestodon*, as well as all lestodontines and  
12  
13 scelidotheriines (Boscaini *et al.* 2019a: char. 370). In *S. uccasamamensis*, the sustentacular  
14  
15 facet is confluent anteriorly with the facet for the cuboid (Fig. 12G), as is typical for  
16  
17 Mylodontinae (McDonald 1987). The facet for the cuboid is anteriorly convex as in most  
18  
19 mylodontids, whereas it is markedly concave in *Nematherium* (YPM-PU 15965) and in the  
20  
21 scelidotheriines (McDonald 1987). The anteriormost portion of the astragalar head of *S.*  
22  
23 *uccasamamensis* bears the articular surface for the navicular (Fig. 11E, F, H). This surface is  
24  
25 flat to slightly concave in *S. uccasamamensis* (Fig. 12E, F, H), as observed in all  
26  
27 mylodontines, whereas in the scelidotheriines this surface is more strongly concave  
28  
29 (McDonald 1987). The intraspecific differences observed in *S. uccasamamensis* in the  
30  
31 surface outline of this facet have been reported for other taxa, like *P. harlani* (Stock 1925),  
32  
33 and directly observed in *T. segnis* (AB, unpub. data).

34  
35  
36  
37  
38  
39  
40 The navicular of *S. uccasamamensis* (Fig. 13A–C) has a typical mylodontine shape, being  
41  
42 broader mediolaterally than deep dorsoventrally. The proximal surface is entirely occupied  
43  
44 by a wide facet for the astragalus (Fig. 13B–C). On the distal surface, a wide elliptical facet  
45  
46 for the ectocuneiform (and probably also for the mesocuneiform) is located along the  
47  
48 ventralmost border (Fig. 13A, C). Adjacent and ventral to the latter facet, on the slender  
49  
50 lateral surface of the bone, there is an anteroposteriorly narrow articulation for the cuboid  
51  
52 (Fig. 13C).

53  
54  
55  
56 The cuboid of *S. uccasamamensis* (Fig. 13D–G) is very similar to the homologous  
57  
58 element in the large-bodied mylodontines such as *G. robustum* and *P. harlani* (Owen 1842;  
59  
60

1  
2  
3 Stock 1925). In proximal view, there is a concave and almost circular facet for the astragalar  
4 head (Fig. 13E, G). The cuboid of *S. uccasamamensis* is delimited anteriorly by an  
5  
6 anteroposteriorly narrow articulation for the navicular (Fig. 13E, G), and posteriorly by a  
7  
8 dorsoventrally enlarged surface for the calcaneum (Fig. 13D). On the distal surface, there are  
9  
10 two facets divided by an oblique ridge, for articulation with mtt5 posteriorly and mtt4  
11  
12 anteriorly (Fig. 13F). Anterodorsally to the latter, there is a smaller rectangular facet for mtt3  
13  
14 that faces anteromedially (Fig. 13G). The cuboid-mtt3 contact is absent in the  
15  
16 scelidotheriines (McDonald 1987). Another difference among mylodontids is the  
17  
18 presence/absence of the cuboid-ectocuneiform contact (Boscaini *et al.* 2019a: char. 376).  
19  
20 This contact is extensive in the scelidotheriines and clearly visible in the articulated pes in  
21  
22 lateral view, whereas it is very reduced in *Pseudoprepothorium* and the lestodontines, and  
23  
24 absent in the other mylodontines such as *G. robustum*, *P. harlani* and *S. uccasamamensis*  
25  
26 (Fig. 13D–I). According to Stock (1925), an extremely reduced cuboid-ectocuneiform facet is  
27  
28 occasionally present in some specimens of *P. harlani*.  
29  
30  
31  
32  
33  
34

35 Therefore, the ectocuneiform of *S. uccasamamensis* (Fig. 13H–I) bears only two large  
36  
37 facets: proximally, a concave surface for the navicular, and distally, a convex surface for  
38  
39 mtt3. This bone is triangular in outline in proximal and distal views, with its longest border  
40  
41 facing laterally. In this regard, it is very similar to the ectocuneiforms of *G. robustum* and *P.*  
42  
43 *harlani* (Stock 1925).  
44  
45  
46

47 The metatarsal series of *S. uccasamamensis* is known from two complete mtt3s, two  
48  
49 incomplete mtt4s and two incomplete mtt5s (Supporting Information, Appendix S1).  
50

51 The mtt3 of *S. uccasamamensis* (Fig. 13J–N) is smaller, in absolute terms, than in any  
52  
53 other mylodontid mtt3, with the exception of *P. garbanii* (UF 10922), which possesses an  
54  
55 mtt3 of similar size. The mtt3 of *S. uccasamamensis* is gracile, with a reduced dorsopalmar  
56  
57 thickness of the shaft in relation to its total length (Boscaini *et al.* 2019a: char. 379), a  
58  
59  
60

1  
2  
3 plesiomorphic morphology that is only observed in *O. grande* among other mylodontid  
4 sloths. Another plesiomorphic feature on the mtt3 of *S. uccasamamensis* is the retention of a  
5 small articular facet for mtt2 (Fig. 13L–M). The mtt2-mtt3 articular surface is generally  
6 absent among Mylodontini (with the exception of *P. garbanii*; UF 10922), though it is  
7 commonly observed among Scelidotheriinae, basal Mylodontinae, and Lestodontini  
8 (Boscaini *et al.* 2109a: char. 378).  
9

10  
11  
12  
13  
14  
15  
16  
17  
18  
19  
20  
21  
22  
23  
24  
25  
26  
27  
28  
29  
30  
31  
32  
33  
34  
35  
36  
37  
38  
39  
40  
41  
42  
43  
44  
45  
46  
47  
48  
49  
50  
51  
52  
53  
54  
55  
56  
57  
58  
59  
60  
Only the proximal portion of mtt4 is available for observation (Fig. 13O–Q). It is smaller  
in size than the homologous element of *G. robustum*, *P. harlani*, *T. segnis* and *L. armatus*,  
resembling more closely that of *O. grande* and *P. garbanii*. A peculiarity of mtt4 in *S.*  
*uccasamamensis* is the reduced facet for mtt5 (Fig. 13Q; Saint-André *et al.* 2010). A similar  
conformation is observed only in *O. grande* among mylodontids, whereas in other members  
of this clade, this facet is more dorsopalmarly elongated.

In lateral view, the mtt5 of *S. uccasamamensis* (Fig. 13R–S) exhibits an arched profile, a  
feature that is plesiomorphic for mylodontids. The arched ventral border of mtt5 is a typical  
feature of Scelidotheriinae. Among Mylodontinae, it is recorded only in *O. grande* and some  
specimens of *T. segnis* (Boscaini *et al.* 2019a: char 382). In proximal view (Fig. 13R), the  
mtt5 of *S. uccasamamensis* possesses unequal articular facets for the cuboid and mtt4, with  
the former consistently larger than the latter.

## DISCUSSION

The postcranial anatomy of *Simomylodon uccasamamensis* was partially described by  
Saint-André *et al.* (2010), but the present study includes many previously undescribed  
elements, and thus allows for a more complete investigation of the postcranial anatomy in  
this taxon. The new data allows for a reconsideration of previously described remains

1  
2  
3 attributed to an “indeterminate Mylodontinae” by Anaya & MacFadden (1995). These  
4  
5 include a partial femur (MNHN-Bol V 3365) and an ungual phalanx (MNHN-Bol V 3355)  
6  
7 from the late Pliocene Bolivian locality of Inchasi. These postcranial remains closely  
8  
9 resemble in both shape and size the material of *S. uccasamamensis* described here, allowing  
10  
11 us to assign these two fossil bones to this taxon.  
12  
13

14  
15 In a similar way, several elements of uncertain attribution recovered from the Casira  
16  
17 Basin and described by Quiñones *et al.* (2019) can be reassigned to *S. uccasamamensis*.  
18  
19 These include the femoral and astragalar specimens JUY-P-0081, JUY-P-0082 and JUY-P-  
20  
21 0089 (Quiñones *et al.* 2019: figs 6–7, 10). In fact, these specimens are morphologically  
22  
23 identical to those presented in this paper, and their dimensions (see Quiñones *et al.* 2019: tab.  
24  
25 2) fall well within the morphometric range of *S. uccasamamensis* (Supporting Information,  
26  
27 Appendix S3). The same can also be said for the mandible JUY-P-0089, which Quiñones *et*  
28  
29 *al.* (2019: fig. 9) recognized as similar to that of *S. uccasamamensis*. Considering this  
30  
31 context, it is also plausible that the remaining mylodontine specimen described by Quiñones  
32  
33 *et al.* (2019), a fragment of a juvenile skull (JUY-P-0173; Quiñones *et al.* 2019: fig. 8) can be  
34  
35 ascribed to *S. uccasamamensis*. However, homologous comparative remains from a similar  
36  
37 developmental stage have not been recovered in the material from the Bolivian Altiplano  
38  
39 (Boscaini *et al.* 2019b), thereby impeding a definitive corroboration.  
40  
41  
42  
43

44  
45 The large sample described in the present study, together with a previous analysis of  
46  
47 craniodental remains (Boscaini *et al.* 2019b), permits now an almost total characterization of  
48  
49 the skeletal anatomy of this species, making *S. uccasamamensis* the best known early  
50  
51 member of Mylodontini. Overall, as noted by Saint-André *et al.* (2010), the postcranial  
52  
53 anatomy of *S. uccasamamensis* closely resembles that of their larger and younger  
54  
55 mylodontine relatives, such as the well-known Pleistocene taxa *Glossotherium robustum* and  
56  
57 *Paramylodon harlani* (Owen 1842; Stock 1925).  
58  
59  
60



1  
2  
3 Indeed, *S. uccasamamensis* already displays some postcranial features that are recovered  
4 as synapomorphies of Mylodontini. These include the flat contour of the astragalar discoid  
5 process in lateral view (Boscaini *et al.* 2019a: char. 369) and the presence of osteoderms  
6 (Boscaini *et al.* 2019a: char. 383). In *S. uccasamamensis*, an agglomeration of small (around  
7 4 mm in average diameter) osteoderms (Fig. 14) was found in association with the skull  
8 MNHN-Bol V 3726 from Casira (Boscaini *et al.* 2019b: fig. 6), and were probably derived  
9 from cranial/neck areas. An isolated, larger (around 17 mm diameter) osteoderm was found  
10 in association with an astragalus from the same locality, and tentatively attributed to *S.*  
11 *uccasamamensis* (Quiñones *et al.* 2019: fig. 10). Given the remarkable variation recognized  
12 in osteoderm shape and size in a single individual, even among dermal ossicles of the same  
13 anatomical region (Brambilla *et al.* 2019), it is plausible that both osteoderms belonged to *S.*  
14 *uccasamamensis*, thus serving to define the size range of these elements for this taxon.  
15 McDonald (2018) suggested that osteoderms may represent an independent acquisition in  
16 some sloth groups, rather than a retained plesiomorphic condition from the common ancestor  
17 of Xenarthra. This view was confirmed by recent reviews (Cartelle *et al.* 2019) and  
18 phylogenetic analyses (Boscaini *et al.* 2019a). Indeed, the presence of osteoderms was  
19 recovered as a synapomorphy of Mylodontini (Boscaini *et al.* 2019a) independently acquired  
20 by the Pleistocene scelidotheriine *Valgipes bucklandi* (Cartelle *et al.* 2019). The oldest prior  
21 record of sloth osteoderms was identified by Rovereto (1914) for *Pleurolestodon*, from the  
22 late Miocene of Argentina, but these fossils are currently missing from the MACN collection  
23 (Curator L. Chornogubsky, pers. comm.). However, isolated dermal ossicles were reported  
24 from coeval sediments of the same region by Nasif *et al.* (2008), thereby confirming that the  
25 earliest known appearance of the character for sloths is at least in the late Miocene. Even if  
26 their attribution is uncertain, they could plausibly be derived from *P. acutidens*. Osteoderms  
27 have not yet been reported in the Pliocene Mylodontini *G. chapadmalense* (Kraglievich 1925;  
28  
29  
30  
31  
32  
33  
34  
35  
36  
37  
38  
39  
40  
41  
42  
43  
44  
45  
46  
47  
48  
49  
50  
51  
52  
53  
54  
55  
56  
57  
58  
59  
60

1  
2  
3 McDonald 2018), but large numbers of osteoderms were recovered for the North American  
4  
5 Pliocene species *P. garbanii* (Robertson 1976; McDonald 2018).  
6  
7

8 For several other postcranial features, *S. uccasamamensis*, together with *P. acutidens* and  
9  
10 *G. chapadmalense*, show plesiomorphic conditions, whereas the derived conditions are  
11  
12 observed in the remaining Mylodontini. For these features, the morphologies observed in *S.*  
13  
14 *uccasamamensis* are more reminiscent of Scelidotheriinae and/or Lestodontini, rather than  
15  
16 Pleistocene Mylodontini such as *G. robustum* and *P. harlani* (Owen 1842; Stock 1925).  
17  
18

19 Primitive features in the postcranial skeleton of *S. uccasamamensis* were identified for the  
20  
21 humerus, radius, ulna, manus, tibia and pes (Boscaini *et al.* 2019a). These include, in the  
22  
23 forelimb, the lack of a proximodistally vertical supinator crest on the humerus, the equally  
24  
25 expanded lateral and medial humeral epicondyles, and the presence of a marked convexity of  
26  
27 the anterior margin of the radius. In the manus, *S. uccasamamensis* shows peculiar trapezoid  
28  
29 proportions and an occasionally-fused magnum and third metacarpal (Saint-André *et al.*  
30  
31 2010). In the hind limb, the tibia is mediolaterally narrow relative to its total length, and  
32  
33 possesses two deep grooves for tendons on the posteromedial margin of the distal tibial  
34  
35 epiphysis. In the pes, *S. uccasamamensis* exhibits a marked sustentacular process of the  
36  
37 calcaneum and a sulcus tali of the astragalus, a relatively gracile third metatarsal which  
38  
39 maintains a contact with the second metatarsal, and a fifth metatarsal showing an arched  
40  
41 ventral profile in lateral view. The presence of these features contributes to the phylogenetic  
42  
43 placement *S. uccasamamensis* at the base of Mylodontini, together with other Neogene taxa  
44  
45 such as *P. acutidens* and *G. chapadmalense* (Boscaini *et al.* 2019a). However, as previously  
46  
47 noted, the postcranium of the latter two taxa is largely unknown.  
48  
49  
50  
51  
52  
53

54 From a morphofunctional point of view, some preliminary, qualitative considerations on  
55  
56 the postcranial elements of *S. uccasamamensis* can be discussed. Some of the distinctive  
57  
58 features recognized in the present study are likely related to paleobiological factors such as  
59  
60

1  
2  
3 digging capabilities and body size. Basically, the proportions and general features of the  
4  
5 appendicular skeleton suggest that this animal was a terrestrial quadruped, without any clear  
6  
7 locomotory specializations, and with a generally graviportal limb morphology (*sensu* Carrano  
8  
9 1999). Given the overall similarity of the appendicular proportions among *S.*  
10  
11 *uccasamamensis* and Pleistocene mylodontids, their center of mass likely occupied an  
12  
13 analogous position (Bargo *et al.* 2000; Vizcaíno *et al.* 2001). Thus, the hind limb would have  
14  
15 served mainly for supporting body mass and providing propulsion during locomotion,  
16  
17 whereas the forelimb could have been more involved in other biological roles, such as  
18  
19 digging and foraging. In this sense, the hind limb is more indicative of stance and locomotory  
20  
21 habits than the forelimb.  
22  
23  
24  
25

26 The femoral greater trochanter in *S. uccasamamensis* is well developed, but it does not  
27  
28 protrude proximally as far as the femoral head, suggesting a wide range of movements. The  
29  
30 great development of the gluteal muscles, evidenced by the entheses development, indicates a  
31  
32 marked stabilization of the hip joint. However, the relatively low position of the greater  
33  
34 trochanter suggests a greater leverage for the gluteal group for femoral abduction (and lateral  
35  
36 rotation of the pelvis during the swing phase of the contralateral limb), and reduced leverage  
37  
38 for limb extension when compared to extant ambulatory herbivores of similar size (e.g., large  
39  
40 bovids and rhinocerotids; Hildebrand & Goslow 2001). The distal epiphysis of the femur in  
41  
42 *S. uccasamamensis* is wide transversely and relatively shallow, with an almost flat patellar  
43  
44 groove connected to asymmetrical femoral condyles, which are broader mediolaterally than  
45  
46 they are deep anteroposteriorly (Fig. 9). This morphology is indicative of a plantigrade  
47  
48 stance, with a more extended knee than in modern, similar-sized herbivores (de Toledo  
49  
50 1998). Proportions of both zeugopodia, which are short relative to the stylopodia, especially  
51  
52 in the hind limb, indicate lower cursorial performance than in similar-sized modern bovids  
53  
54 (de Toledo 1998).  
55  
56  
57  
58  
59  
60

1  
2  
3 A preliminary body weight estimation for *S. uccasamamensis* was calculated using  
4 allometric equations established by Fariña *et al.* (1998) and Toledo *et al.* (2014). The value  
5 obtained of about 370 kg, together with the general proportions of the limbs, allow us to  
6 exclude arboreality as a locomotory mode for *S. uccasamamensis*. Nevertheless, the bulky  
7 musculature that surely powered this animal, and the great development of entheses, could  
8 have allowed occasional climbing of rocks or trunks, as seen in similarly-sized living animals  
9 such as bears and large felids (Hildebrand & Goslow 2001). The climbing performance of *S.*  
10 *uccasamamensis* likely was that of a slow and cautious animal. On the other hand, its body  
11 mass estimate is far less than that of other representatives of Mylodontinae, making this  
12 species one of the smallest members of a group characterized by many gigantic forms (AB,  
13 unpub. data). Accordingly, some primitive features of *Simomylodon* can be tentatively  
14 attributed to the absence of adaptations for supporting a gigantic body mass. For instance,  
15 fusion or simplification of joint surfaces, as described in larger mylodontids such as *G.*  
16 *robustum* and *P. harlani* (e.g., Owen 1842; Stock 1925; Cartelle *et al.* 2019) are not  
17 observed. Metatarsals are more gracile and elongated, resulting in a wider and less compact  
18 pes than in *Paramylodon* or *Lestodon*.

19  
20  
21 Since most extinct and extant xenarthrans exhibit clear specializations for digging, with  
22 the notable exception of extant sloths, it is likely that morphologies related to fossoriality are  
23 primitive for the sloth lineage and particularly developed in mylodontids (Pujos *et al.* 2012;  
24 Gaudin & Croft 2015). In this sense, the general morphology of *S. uccasamamensis* is  
25 consistent with a certain degree of digging capability, as in many other Mylodontidae.  
26 However, in this taxon, humeral and ulnar entheses are less developed, the olecranon is less  
27 elongated, and autopodial elements are less bulky than in *Glossotherium* and *Scelidotherium*,  
28 a suite of postcranial features underscoring the absence of strong digging specialization in  
29 *Simomylodon*. For this reason, *S. uccasamamensis* was probably not an active digger, and  
30  
31  
32  
33  
34  
35  
36  
37  
38  
39  
40  
41  
42  
43  
44  
45  
46  
47  
48  
49  
50  
51  
52  
53  
54  
55  
56  
57  
58  
59  
60

1  
2  
3 was likely not a cave excavator, as has been inferred for some Pleistocene South-American  
4 mylodontids (Bargo *et al.* 2000; Vizcaíno *et al.* 2001). Burrowing habits in Pleistocene  
5 mylodontid sloths from the southern cone was a probable strategy to escape predation from  
6 large carnivores, which entered from North into South America during the Great American  
7 Biotic Interchange (Vizcaíno *et al.* 2001; Woodburne *et al.* 2010). So far, neither large-sized  
8 cave systems, nor fossil remains of North American putative predators have been recovered  
9 in the Pliocene of the Bolivian Altiplano (Marshall *et al.* 1983; Hoffstetter 1986; Marshall &  
10 Sempéré 1991; Anaya & MacFadden 1995). This suggests that the digging abilities of *S.*  
11 *uccasamamensis* were more likely related to foraging than to a defence strategy.  
12  
13  
14  
15  
16  
17  
18  
19  
20  
21  
22  
23  
24  
25

## 26 CONCLUSIONS

27  
28  
29  
30 The newly documented postcranial elements of *Simomylodon uccasamamensis*  
31 substantially increase our knowledge of the anatomy and inferred locomotory behavior of this  
32 extinct sloth, which was a common faunal element in the late Miocene–late Pliocene deposits  
33 of the Bolivian Altiplano. The appendicular skeleton of *S. uccasamamensis* is reminiscent of  
34 that of larger Pleistocene relatives, such as *Glossotherium robustum* and *Paramylodon*  
35 *harlani*. However, some features are also shared with the postcrania of scelidotheriine and  
36 lestodontine sloths, and contribute to placing *S. uccasamamensis* in a relatively basal position  
37 among Mylodontini. Thanks to its remarkable skeletal completeness, *S. uccasamamensis*  
38 represents the best known early member of Mylodontini, and a key taxon for understanding  
39 the evolution of the entire clade. General morphology of both the forelimb and the hind limb  
40 of *S. uccasamamensis* indicate that this medium-sized mammal was engaged in a form of  
41 terrestrial quadrupedalism, with a graviportal aspect, including moderate climbing and  
42 digging abilities in its locomotor repertoire. The abundance of skeletal remains of *S.*  
43  
44  
45  
46  
47  
48  
49  
50  
51  
52  
53  
54  
55  
56  
57  
58  
59  
60

1  
2  
3 *uccasamamensis* in several Bolivian localities reflects the widespread geographic distribution  
4  
5 and ecological importance of this taxon in the Pliocene of the Andean Altiplano.  
6  
7  
8  
9

10 *Acknowledgments.* We thank R.D.E. MacPhee, J.J. Flynn, J. Galkin and M. Rios-Dickson  
11  
12 (AMNH), B.J. MacFadden, J.I. Bloch and R.C. Hulbert, Jr. (FLMNH), K.D. Angielczyk, W.  
13  
14 Simpson and A. Stroup (FMNH), L. Chornogubsky, M. Ezcurra, A. Kramarz, P. Teta, G.  
15  
16 Cassini and S. Lucero (MACN), M.A. Reguero, S.C. Scarano and M.L. de los Reyes (MLP),  
17  
18 C. de Muizon and G. Billet (MNHN), K. Seymour (ROM), A. Rincón (IVIC) and R. Sánchez  
19  
20 (AMU-CURS), who kindly gave access to the specimens under their care. We also want to  
21  
22 thank J.V. Tejada-Lara and M. Ubilla for sharing photographs of some fossil specimens. This  
23  
24 paper greatly benefited from thoughtful comments and accurate revisions by Prof. G. De  
25  
26 Iuliis, an anonymous reviewer and the Editor S. Thomas. The data collection for the present  
27  
28 study was greatly facilitated by funding from the FMNH, the AMNH, the FLMNH and the  
29  
30 University of Tennessee at Chattanooga. This research was made possible thanks to the  
31  
32 cooperation agreement between the MNHN-Bol, the IANIGLA and the ISEM (CONICET  
33  
34 Cooperation Agreement N°864/2014), and actively funded by the cooperative programme  
35  
36 ECOS-FonCyT (A14U01) and the National Geographic Society (projects NGS 9971-16 and  
37  
38 EC-44712R-18).  
39  
40  
41  
42  
43  
44  
45  
46  
47

#### 48 **DATA ARCHIVING STATEMENT**

49  
50 Data for this study are available in the Dryad Digital Repository:

51  
52 <https://datadryad.org/stash/share/loTnzKIgnPeYYFn9CGQI8U9FLNVla3j9qcOmQo>

53  
54 [XfkWI](#)

55  
56  
57 Appendix S1. *Simomyiodon uccasamamensis* – Referred material

58  
59 Appendix S2. Comparison taxa – List of observed specimens  
60

Appendix S3. *Simomylodon uccasamamensis* – Measurements

## REFERENCES

- AMSON, E., ARGOT, C., McDONALD, H.G. and DE MUIZON, C. 2015a. Osteology and functional morphology of the forelimb of the marine sloth *Thalassocnus* (Mammalia, Tardigrada). *Journal of Mammalian Evolution*, **22**, 169–242.
- , ---, ---, --- 2015b. Osteology and functional morphology of the hind limb of the marine sloth *Thalassocnus* (Mammalia, Tardigrada). *Journal of Mammalian Evolution*, **22**, 355–419.
- ANAYA, F. and MacFADDEN, B.J. 1995. Pliocene mammals from Inchasi, Bolivia: the endemic fauna just before the Great American Interchange. *Bulletin of the Florida Museum of Natural History*, **39**, 87–140.
- BARGO, M.S., VIZCAÍNO, S.F., ARCHUBY, F.M. and BLANCO, R.E. 2000. Limb bone proportions, strength and digging in some Lujanian (Late Pleistocene-Early Holocene) mylodontid ground sloths (Mammalia: Xenarthra). *Journal of Vertebrate Paleontology*, **20**, 601–610.
- BOSCAINI, A., PUJOS, F., GAUDIN, T.J. 2019a. A reappraisal of the phylogeny of Mylodontidae (Mammalia, Xenarthra) and the divergence of mylodontine and lestodontine sloths. *Zoologica Scripta*, **48**, 691–710.
- , GAUDIN, T.J., MAMANI QUISPE, B., MÜNCH, P., ANTOINE, P-O. and PUJOS, F. 2019b. New well-preserved craniodental remains of *Simomylodon uccasamamensis* (Xenarthra: Mylodontidae) from the Pliocene of the Bolivian Altiplano: phylogenetic, chronostratigraphic and palaeobiogeographical implications. *Zoological Journal of the Linnean Society*, **185**, 459–486.

- 1  
2  
3 ---, ---, TOLEDO, N., MAMANI QUISPE, B., ANTOINE, P-O. and PUJOS, F. 2019c. The  
4 earliest well-documented occurrence of sexual dimorphism in extinct sloths:  
5 evolutionary and palaeoecological insights. *Zoological Journal of the Linnean*  
6 *Society*, **187**, 229–239.  
7  
8  
9  
10  
11  
12 BRAMBILLA, L., TOLEDO, M.J., HARO, J.A. and AGUILAR, J.L. 2019. New osteoderm  
13 morphotype (xenarthra, mylodontidae) from the middle pleistocene of Argentina.  
14 *Journal of South American Earth Sciences*, **95**, 102298.  
15  
16  
17  
18  
19 CARRANO, M.T. 1999. What, if anything, is a cursor? Categories versus continua for  
20 determining locomotor habit in mammals and dinosaurs. *Journal of Zoology*, **247**, 29–  
21 42.  
22  
23  
24  
25  
26 CARTELLE, C. 1980. Estudo comparativo do rádio e esqueleto da mão de *Glossotherium*  
27 (*Ocnotherium*) *giganteum* Lund, 1842. *Anais da Academia Brasileira de Ciências*, **52**,  
28 359–377.  
29  
30  
31  
32  
33 ---, DE IULIIS, G., BOSCAINI, A. and PUJOS, F. 2019. Anatomy, possible sexual  
34 dimorphism, and phylogenetic affinities of a new mylodontine sloth from the Late  
35 Pleistocene of intertropical Brazil. *Journal of Systematic Palaeontology*, **23**, 1957–  
36 1988.  
37  
38  
39  
40  
41  
42 COPE, E.D. 1889. The Edentata of North America. *American Naturalist*, **23**, 657–664.  
43  
44  
45 DE IULIIS, G., BOSCAINI, A., PUJOS, F., McAFEE, R.K., CARTELLE, C., TSUJI, L.J.S.  
46 and ROOK, L. In press. On the status of the giant mylodontine sloth *Glossotherium*  
47 *wegneri* (Xenarthra, Folivora) from the Late Pleistocene of Ecuador. *Comptes rendus*  
48 *Palevol.*  
49  
50  
51  
52  
53  
54 DE TOLEDO, P.M. 1998. *Locomotory patterns within the Pleistocene sloths*. Museu  
55 Paraense Emílio Goeldi, Belém, 192 pp.  
56  
57  
58  
59  
60



- 1  
2  
3 DELSUC, F., CATZEFLIS, F.M., STANHOPE, M.J. and DOUZERY, E.J.P. 2001. The  
4  
5 evolution of armadillos, anteaters and sloths depicted by nuclear and mitochondrial  
6  
7 phylogenies: implications for the status of the enigmatic fossil *Eurotamandua*.  
8  
9 *Proceedings of the Royal Society B*, **268**, 1605–1615.
- 10  
11  
12 ---, KUCH, M., GIBB, G.C., KARPINSKI, E., HACKENBERGER, D., SZPAK, P.,  
13  
14 MARTÍNEZ, J.G., MEAD, J.I., McDONALD, H.G., MacPHEE, R.D.E., BILLET,  
15  
16 G., HAUTIER, L. and POINAR, H.N. 2019. Ancient mitogenomes reveal the  
17  
18 evolutionary history and biogeography of sloths. *Current Biology*, **29**, 2031–2042.
- 19  
20  
21 ENGELMANN, G.F. 1985. The phylogeny of the Xenarthra. 51–64. In MONTGOMERY, G.  
22  
23 G. (ed.) *The evolution and Ecology of Armadillos, Sloths and Vermilinguas*.  
24  
25 Smithsonian Institution Press, Washington, DC, and London, UK, 451 pp.
- 26  
27  
28 EVANS, H.E. and DE LAHUNTA, A. 2013. *Miller's Anatomy of the Dog*. 4<sup>th</sup> edn. Elsevier,  
29  
30 St. Louis. 850 pp.
- 31  
32  
33 FARIÑA, R.A., VIZCAÍNO, S.F. and BARGO, M.S. 1998. Body mass estimations in  
34  
35 Lujanian (Late Pleistocene–Early Holocene of South America) mammal megafauna.  
36  
37 *Mastozoología Neotropical*, **5**, 87–108.
- 38  
39  
40 FLOWER, W.H. 1883. On the arrangement of the orders and families of existing Mammalia.  
41  
42 *Proceedings of the Zoological Society of London*, **51**, 178–186.
- 43  
44  
45 GAUDIN, T.J. 2004. Phylogenetic relationships among sloths (Mammalia, Xenarthra,  
46  
47 Tardigrada): the craniodental evidence. *Zoological Journal of the Linnean Society*,  
48  
49 **140**, 255–305.
- 50  
51  
52 GAUDIN, T.J. and CROFT, D.A. 2015. Paleogene Xenarthra and the evolution of South  
53  
54 American mammals. *Journal of Mammalogy*, **96**, 622–634.
- 55  
56  
57 GERVAIS, P. 1873. Mémoire sur plusieurs espèces de Mammifères fossiles propres à  
58  
59 l'Amérique méridionale. *Mémoires de la Société Géologique de France*, **9**, 1–44.  
60

- 1  
2  
3 GILL, T. 1872. Arrangement of the families of mammals, with analytical tables. *Smithsonian*  
4  
5 *Miscellaneous Collections*, **11**, 1–98.  
6  
7  
8 HARO, J.A., TAUBER, A.A. and KRAPOVICKAS, J.M. 2016. The manus of *Mylodon*  
9  
10 *darwinii* Owen (Tardigrada, Mylodontidae) and its phylogenetic implications. *Journal*  
11  
12 *of Vertebrate Paleontology*, **36**, e1188824.  
13  
14  
15 HILDEBRAND, M. and GOSLOW, G. 2001. *Analysis of vertebrate structure*. 5<sup>th</sup> edn.  
16  
17 Wiley, New York, NY, 635 pp.  
18  
19 HIRSCHFELD, S.E. 1985. Ground sloths from the Friasian La Venta Fauna, with additions  
20  
21 to the Pre-Friasian Coyaima Fauna of Colombia, South America. *University of*  
22  
23 *California Publications in Geological Sciences*, **128**, 1–91.  
24  
25  
26 HOFFSTETTER, R. 1986. High andean mammalian faunas during the Plio-Pleistocene. 219–  
27  
28 245. In VUILLEUMIER, F. and MONASTERIO, M. (eds). *High altitude tropical*  
29  
30 *biogeography*. New York, NY, 649 pp.  
31  
32  
33 KRAGLIEVICH, L. 1925. Cuatro nuevos Gravígrados de la fauna araucana chapadmalense.  
34  
35 *Anales del Museo Nacional de Historia Natural "Bernardino Rivadavia"*, **33**, 215–  
36  
37 235.  
38  
39  
40 --- 1926. Notas sobre gravígrados de Sud América. I. Indicios de evolución progresiva en dos  
41  
42 astrágalos y un calcáneo de *Megatherium*. *Anales del Museo Nacional de Historia*  
43  
44 *Natural de Buenos Aires*, **34**, 21–29.  
45  
46  
47 MARIOTTI, V., FACCHINI, F. and BELCASTRO, M.G. 2007. The study of entheses:  
48  
49 proposal of a standardised scoring method for twenty-three entheses of the postcranial  
50  
51 skeleton. *Collegium antropologicum*, **31**, 291–313.  
52  
53  
54 MARSHALL, L.G. and SEMPÉRÉ, T. 1991. The Eocene to Pleistocene vertebrates of  
55  
56 Bolivia and their stratigraphic context: a review. 631–652. In SUÁREZ-SORUCO, R.  
57  
58  
59  
60

- 1  
2  
3 (ed.). *Fósiles y facies de Bolivia – Vol. I Vertebrados*. Yacimientos Petrolíferos  
4  
5 Fiscales Bolivianos, Santa Cruz, Bolivia, 359 pp.  
6  
7  
8 ---, HOFFSTETTER, R. and PASCUAL, R. 1983. Mammals and stratigraphy:  
9  
10 geochronology of the continental mammal-bearing Tertiary of South America.  
11  
12 *Palaeovertebrata (Mémoire Extraordinaire)*: 1–93.  
13  
14  
15 McAFEE, R.K. 2016. Description of new postcranial elements of *Myiodon darwinii* Owen  
16  
17 1839 (Mammalia: Pilosa: Mylodontinae), and functional morphology of the forelimb.  
18  
19 *Ameghiniana*, **53**, 418–443.  
20  
21  
22 McDONALD, H.G. 1977. *Description of the osteology of the extinct gravi-grade edentate,*  
23  
24 *Megalonyx, with observations on its ontogeny, phylogeny and functional anatomy.*  
25  
26 Unpublished Master thesis, University of Florida, Gainesville, 328 pp.  
27  
28  
29 --- 1987. *A systematic review of the Plio-Pleistocene scelidotheriine ground sloths*  
30  
31 *(Mammalia: Xenarthra: Mylodontidae)*. Unpublished PhD Thesis, University of  
32  
33 Toronto, Toronto, 478 pp.  
34  
35  
36 --- 2003. Xenarthran skeletal anatomy: primitive or derived? (Mammalia, Xenarthra).  
37  
38 *Senckenbergiana biologica*, **83**, 5–18.  
39  
40  
41 --- 2018. An overview of the presence of osteoderms in sloths: implications for osteoderms as  
42  
43 a plesiomorphic character of the Xenarthra. *Journal of Mammalian Evolution*, **25**,  
44  
45 485–493.  
46  
47  
48 --- and DE IULIIS, G. 2008. Fossil history of sloths. 39–55. In VIZCAÍNO, S. F. and  
49  
50 LOUGHRY, W. J. (eds). *The Biology of the Xenarthra*. The University of Florida  
51  
52 Press, Gainesville, FL, 370 pp.  
53  
54  
55 McKENNA, M.C. and BELL, S.K. 1997. *Classification of Mammals above the Species*  
56  
57 *Level*. Columbia University Press, New York, NY. 631 pp.  
58  
59  
60

- 1  
2  
3 MEREDITH, R.W., JANEČKA, J.E., GATESY, J., RYDER, O.A., FISHER, C.A.,  
4  
5 TEELING, E.C., GOODBLA, A., EIZIRIK, E., SIMÃO, T.L.L., STADLER, T.,  
6  
7 RABOSKY, D.L., HONEYCUTT, R.L., FLYNN, J.J., INGRAM, C.M., STEINER,  
8  
9 C., WILLIAMS, T.L., ROBINSON, T.J., BURK-HERRICK, A., WESTERMAN, M.,  
10  
11 AYOUB, N.A., SPRINGER, M.S. and MURPHY, W.J. 2011. Impacts of the  
12  
13 Cretaceous terrestrial revolution and KPg extinction on mammal diversification.  
14  
15 *Science*, **334**, 521–524.  
16  
17  
18  
19 MONTELLANO-BALLESTEROS, M. and CARRANZA-CASTAÑEDA, Ó. 1986.  
20  
21 Descripción de un milodóntido del Blancano temprano de La Mesa Central de  
22  
23 México. *Universidad Nacional Autónoma de Mexico, Instituto de Geología, Revista*,  
24  
25 **6**, 193–203.  
26  
27  
28  
29 NASIF, N.L., ESTEBAN, G. and GEORGIEFF, S.M. 2008. Nuevo registro de vertebrados  
30  
31 para la Formación Aconquija, provincia de Catamarca, Noroeste de Argentina.  
32  
33 Implicancias cronoestratigráficas y consideraciones paleoambientales. *Acta Geologica*  
34  
35 *Lilloana*, **20**, 99–112.  
36  
37  
38 O'LEARY, M.A., BLOCH, J.I., FLYNN, J.J., GAUDIN, T.J., GIALLOMBARDO, A.,  
39  
40 GIANNINI, N.P., GOLDBERG, S.L., KRAATZ, B.P., LUO, Z-X., MENG, J., NI,  
41  
42 X., NOVACEK, M.J., PERINI, F.A., RANDALL, Z.S., ROUGIER, G.W., SARGIS,  
43  
44 E.J., SILCOX, M.T., SIMMONS, N.B., SPAULDING, M., VELAZCO, P.M.,  
45  
46 WEKSLER, M., WIBLE, J.R. and CIRRANELLO, A.L. 2013. The placental  
47  
48 mammal ancestor and the post–K-Pg radiation of placentals. *Science*, **339**, 662–667.  
49  
50  
51 OWEN, R. 1842. *Description of the skeleton of an extinct gigantic sloth, Mylodon robustus,*  
52  
53 *Owen with observations on the osteology, natural affinities, and probable habits of*  
54  
55 *the megatheroid quadrupeds in general.* R. & J.E. Taylor, London, 176 pp.  
56  
57  
58  
59  
60

- 1  
2  
3 PITANA, V.G. 2011. *Estudo do gênero Glossotherium Owen, 1840 (Xenarthra, Tardigrada,*  
4 *Mylodontidae), Pleistoceno do Estado do Rio Grande do Sul, Brasil.* Unpublished  
5  
6 Master Thesis, Universidade Federal do Rio Grande do Sul, Porto Alegre, 183 pp.  
7  
8  
9  
10 PRESSLEE, S., SLATER, G.J., PUJOS, F., FORASIEPI, A.M., FISCHER, R., MOLLOY,  
11  
12 K., MACKIE, M., OLSEN, J.V., KRAMARZ, A., TAGLIORETTI, M., SCAGLIA,  
13  
14 F., LEZCANO, M., LANATA, J.L., SOUTHON, J., FERANEC, R., BLOCH, J.,  
15  
16 HAJDUK, A., MARTIN, F.M., SALAS GISMONDI, R., REGUERO, M., DE  
17  
18 MUIZON, C., GREENWOOD, A., CHAIT, B.T., PENKMAN, K., COLLINS, M.,  
19  
20 MacPHEE, R.D.E. 2019. Palaeoproteomics resolves sloth relationships. *Nature*  
21  
22 *Ecology & Evolution*, **3**, 1121–1130.  
23  
24  
25  
26 PUJOS, F. and DE IULIIS, G. 2007. Late Oligocene Megatherioidea Fauna (Mammalia:  
27  
28 Xenarthra) from Salla–Luribay (Bolivia): new data on basal sloth radiation and  
29  
30 Cingulata–Phyllophaga split. *Journal of Vertebrate Paleontology*, **27**, 132–144.  
31  
32  
33 ---, GAUDIN, T.J., DE IULIIS, G. and CARTELLE, C. 2012. Recent advances on  
34  
35 variability, morpho-functional adaptations, dental terminology, and evolution of  
36  
37 sloths. *Journal of Mammalian Evolution*, **19**, 159–169.  
38  
39  
40 ---, DE IULIIS, G. and CARTELLE, C. 2017. A paleogeographic overview of tropical fossil  
41  
42 sloths: towards an understanding of the origin of extant suspensory sloths? *Journal of*  
43  
44 *Mammalian Evolution*, **24**, 19–38.  
45  
46  
47 QUIÑONES, S.I., MIÑO-BOILINI, Á.R., ZURITA, A.E., CONTRERAS, S.A., LUNA,  
48  
49 C.A., CANDELA, A.M., CAMACHO, M., ERCOLI, M.D., SOLÍS, N. and  
50  
51 BRANDONI, D. 2019. New records of Neogene Xenarthra (Mammalia) from eastern  
52  
53 Puna (Argentina): diversity and biochronology. *Journal of Paleontology*, **93**, 1258–  
54  
55 1275.  
56  
57  
58 RAUTENBERG, M. 1906. Über *Pseudolestodon hexaspondylus*. *Palaeontographica*,  
59  
60

1  
2  
3 **53**, 1–50.  
4

5 RINCÓN, A.D., SOLÓRZANO, A., McDONALD, H.G. and FLORES, M.N. 2016.  
6

7 *Baraguatherium takumara*, gen. et sp. nov., the earliest mylodontoid sloth (Early  
8 Miocene) from northern South America. *Journal of Mammalian Evolution*, **24**, 179–  
9  
10  
11  
12 191.  
13

14 ROBERTSON, J.S. 1976. Latest Pliocene mammals from Haile XV A, Alachua County,  
15 Florida. *Bulletin of the Florida Museum of Natural History*, **20**, 111–186.  
16

17 ROSE, K.D. and EMRY, R.J. 1993. Relationships of Xenarthra, Pholidota, and fossil  
18 “edentates”: the morphological evidence. 81–102. In SZALAY, F.S., NOVACEK,  
19 M.J. and McKENNA, M.C. (eds.) *Mammal Phylogeny: Placentals*. Springer, New  
20  
21  
22  
23  
24  
25  
26  
27  
28  
29  
30  
31  
32  
33  
34  
35  
36  
37  
38  
39  
40  
41  
42  
43  
44  
45  
46  
47  
48  
49  
50  
51  
52  
53  
54  
55  
56  
57  
58  
59  
60  
York, NY, 321 pp.

ROVERETO, C. 1914. Los estratos araucanos y sus fósiles. *Anales del Museo Nacional de*  
*Buenos Aires*, **25**, 1–249.

SAINT-ANDRÉ, P-A. 1994. *Contribution à l'étude des grands mammifères du Néogène de*  
*l'altiplano bolivien*. Unpublished PhD Thesis, Museum national d'Histoire naturelle  
de Paris, Paris, 664 pp.

SAINT-ANDRÉ, P-A., PUJOS, F., CARTELLE, C., DE IULIIS, G., GAUDIN, T.J.,  
McDONALD, H.G. and MAMANI QUISPE, B. 2010. Nouveaux paresseux terrestres  
(Mammalia, Xenarthra, Mylodontidae) du Néogène de l'Altiplano bolivien.  
*Geodiversitas*, **32**, 255–306.

SHOCKEY, B.J. and ANAYA, F. 2011. Grazing in a new late Oligocene mylodontid sloth  
and a mylodontid radiation as a component of the Eocene–Oligocene faunal turnover  
and the early spread of grasslands/savannas in South America. *Journal of Mammalian*  
*Evolution*, **18**, 101–115.

- 1  
2  
3 STOCK, C. 1925. Cenozoic gravi-grade Edentates of Western North America with special  
4 reference to the Pleistocene Megalonychinae, and Mylodontidae of Rancho La Brea.  
5 *Carnegie Institution of Washington, Publications*, **331**, 1–206.  
6  
7  
8  
9  
10 TOLEDO, N., BARGO, M.S. and VIZCAÍNO, S.F. 2013. Muscular reconstruction and  
11 functional morphology of the forelimb of early Miocene sloths (Xenarthra, Folivora)  
12 of Patagonia. *The Anatomical Record*, **296**, 305–325.  
13  
14  
15  
16  
17 ---, CASSINI, G.H., VIZCAÍNO, S.F. and BARGO, M.S. 2014. Mass estimation of  
18 Santacrucian sloths from the Early Miocene Santa Cruz Formation of Patagonia,  
19 Argentina. *Acta Palaeontologica Polonica*, **59**, 267–280.  
20  
21  
22  
23  
24 ---, BARGO, M.S. and VIZCAÍNO, S.F. 2015. Muscular reconstruction and functional  
25 morphology of the hind limb of santacrucian (early Miocene) sloths (Xenarthra,  
26 Folivora) of Patagonia. *The Anatomical Record*, **298**, 842–864.  
27  
28  
29  
30  
31 VARELA, L., TAMBUSO, P.S., McDONALD, H.G. and FARIÑA, R.A. 2018. Phylogeny,  
32 macroevolutionary trends and historical biogeography of sloths: insights from a  
33 Bayesian morphological clock analysis. *Systematic Biology*, **68**, 204–218.  
34  
35  
36  
37  
38 VARGAS-PEIXOTO, D., COLUSSO, C.S., DA-ROSA, Á.A.S. and KERBER, L. 2019. A  
39 new record of *Lestodon armatus* Gervais 1855 (Xenarthra, Mylodontidae) from the  
40 Quaternary of southern Brazil and remarks on its postcranial anatomy. *Historical*  
41 *Biology*, published online 2 April 2019. doi:10.1080/08912963.2019.1597075  
42  
43  
44  
45  
46  
47 VIZCAÍNO, S.F., ZÁRATE, M., BARGO, M.S. and DONDAS, A. 2001. Pleistocene  
48 burrows in the Mar del Plata area (Argentina) and their probable builders. *Acta*  
49 *Palaeontologica Polonica*, **46**, 289–301.  
50  
51  
52  
53  
54 WEBB, S.D. 1989. Osteology and relationships of *Thinobadistes segnis*, the first mylodont  
55 sloth in North America. 469–532. In REDFORD, K.H. and EISENBERG, J.F. (eds.)  
56 *Advances in Neotropical Mammalogy*. Sandhill Crane Press, Gainesville, FL, 614 pp.  
57  
58  
59  
60

1  
2  
3 WINGE, H. 1915. *Jordfundne og nulevende Gumlere (Edentata) fra Lagoa Santa, Minas*  
4  
5 *Geraes, Brasilien*. Bianco Lunos, Copenhagen, 321 pp.

6  
7  
8 WOODBURNE, M.O. 2010. The great american biotic interchange: dispersals, tectonics,  
9  
10 climate, sea level and holding pens. *Journal of Mammalian Evolution*, **17**, 245–264.

11  
12  
13  
14  
15 **FIGURE CAPTIONS**

16  
17  
18  
19 **FIG. 1.** Map of the late Neogene fossil-bearing localities of Bolivia in which the remains of  
20  
21 the mylodontid sloth *Simomylodon uccasamamensis* have been recovered. Circles: cities;  
22  
23 Stars: fossil localities.

24  
25  
26 [Suggested size: two-thirds page width]

27  
28  
29  
30  
31 **FIG. 2.** Left scapula of the mylodontid sloth *Simomylodon uccasamamensis* (MNHN-Bol V  
32  
33 3718) in lateral (A), proximal (B) and medial (C) views. Abbreviations: ap, acromion  
34  
35 process; cf, clavicular fossa; cop, coracoid process; csf, coraco-scapular foramen; gc, glenoid  
36  
37 cavity; isf, infraspinous fossa; por, posterior ridge of subscapular fossa; psf, post-scapular  
38  
39 fossa; scs, secondary spine; ssf, supraspinous fossa; ssp, spine of scapula. Scale bar equals 5  
40  
41 cm.

42  
43  
44 [Suggested size: two-thirds page width]

45  
46  
47  
48  
49 **FIG. 3.** Right humerus of the mylodontid sloth *Simomylodon uccasamamensis* (MNHN-Bol  
50  
51 V 13367) in proximal (A), anterior (B) and distal (C) views. Abbreviations: aer, ascending  
52  
53 entepicondylar ridge; cpt, capitulum; dc, deltoid crest; gt, greater tuberosity; hh, humeral  
54  
55 head; lep, lateral epicondyle; lt, lesser tuberosity; mep, medial epicondyle; scr, supinator  
56  
57 crest, tr, trochlea. Scale bar equals 5 cm.



[Suggested size: single column]

**FIG. 4.** Right radius of the mylodontid sloth *Simomylodon uccasamamensis* (MNHN-Bol V 3375) in anterior (A), lateral (B), posterior (C), medial (D), proximal (E) and distal (F) views. Abbreviations: cpf, capitular facet; luf, lunar facet; psp, pseudostyloid process; prr, pronator ridge; puf, proximal ulnar facet; rtu, radial tuberosity; scf, scaphoid facet; stp, styloid process; un, ulnar notch. Scale bar equals 5 cm.

[Suggested size: full page width]

**FIG. 5.** Proximal fragment of left ulna of the mylodontid sloth *Simomylodon uccasamamensis* (MNHN-Bol V 3717) in anterior (A), lateral (B) and posterior (C) views. Abbreviations: ancp, anconeal process; cp, coronoid process; olec, olecranon; pm, posterior margin; rn, radial notch; tn(lp), trochlear notch (lateral portion); tn(mp), trochlear notch (medial portion). Scale bar equals 5 cm.

[Suggested size: two-thirds page width]

**FIG. 6.** Carpals (A-P) and sesamoids (Q-T) of the mylodontid sloth *Simomylodon uccasamamensis*. A-B, left scaphoid (MNHN.F.AYO180) in distal (A) and dorsal (B) views; C-E, left lunar (MNHN.F.AYO111) in anterior (C), dorsal (D) and distal (E) views; F-H, left cuneiform (MNHN.F.AYO109) in proximal (F), dorsal (G) and distal (H) views; I-K, left trapezoid (MNHN.F.AYO180) in proximal (I), posterior (J) and distal (K) views; L-N, right unciform (MNHN-Bol V 12953) in proximal (L), dorsal (M) and distal (N) views; O-P, right pisiform (MNHN.F.AYO180) in palmar (O) and oblique-palmar (P) views; Q-R, right medial sesamoid of mtc4 (MNHN.F.AYO114) in medial (Q) and lateral (R) views; S-T, right lateral sesamoid of mtc4 (MNHN.F.AYO111) in medial (S) and palmar (T) views. Black and white

1  
2  
3 photos have been taken from St-André et al. (2010). Abbreviations refer to articular facets for  
4 the indicated bones, as follows: cmc, carpal-metacarpal complex; cu, cuneiform, lu, lunar;  
5 mg, magnum; mtc (2-3-4-5), metacarpal (2-3-4-5); pis, pisiform; rd, radius; sc, scaphoid; td,  
6 trapezoid; ul, ulna; un, unciform. Scale bar equals 2 cm.  
7  
8  
9  
10

11 [Suggested size: full page width]  
12  
13  
14  
15  
16

17 **FIG. 7.** Metacarpal elements of the mylodontid sloth *Simomylodon uccasamamensis*. A-B,  
18 right carpal-metacarpal complex (MNHN.F.VIZ32) in dorsal (A) and distal (B) views; C-E,  
19 right metacarpal II (MNHN.F.AYO190) in anterior (C), posterior (D) and proximal (E)  
20 views; F-H, right metacarpal III (MNHN.F.VIZ27) in dorsal (F), palmar (G) and proximal  
21 (H) views; I-M, left metacarpal III fused with magnum (MNHN.F.AYO179) in proximal (I),  
22 dorsal (J), posterior (K), palmar (L) and anterior (M) views; N-P, proximal fragment of left  
23 metacarpal IV (MNHN.F.VIZ33) in proximal (N), dorsal (O) and posterior (P) views; Q-S,  
24 left metacarpal V (MNHN-Bol V 13367) in anterior (Q), dorsal (R) and distal (S) views.  
25  
26  
27  
28  
29  
30  
31  
32  
33  
34

35 Abbreviations refer to articular facets for the indicated bones, as follows: cmc, carpal-  
36 metacarpal complex; lu, lunar; mg, magnum; mtc (2-3-4-5), metacarpal (2-3-4-5); pp (1-2-3-  
37 5), proximal phalanx (1-2-3-5); sc, scaphoid; td, trapezoid; un, unciform. Scale bar equals 2  
38 cm.  
39  
40  
41  
42  
43  
44

45 [Suggested size: full page width]  
46  
47  
48  
49

50 **FIG. 8.** Manual phalanges of the mylodontid sloth *Simomylodon uccasamamensis*. A-C, right  
51 proximal phalanx of third digit (MNHN-Bol V 3313) in proximal (A), lateral (B) and distal  
52 (C) views; D-G, right intermediate phalanx of third digit (MNHN-Bol V 3313) in proximal  
53 (D), lateral (E), dorsal (F) and palmar (G) views; H-J, left ungual phalanx of first digit  
54 (MNHN.F.AYO180) in dorsal (H), medial (I) and palmar (J) views; K-M, left ungual phalanx  
55  
56  
57  
58  
59  
60

1  
2  
3 of second digit (MNHN.F.AYO180) in dorsal (K), medial (L) and palmar (M) views; N-P,  
4 left ungual phalanx of third digit (MNHN.F.AYO180) in dorsal (N), medial (O) and palmar  
5 (P) views. Scale bar equals 2 cm.  
6  
7

8  
9  
10 [Suggested size: full page width]  
11  
12  
13

14  
15 **FIG. 9.** Right femur of the mylodontid sloth *Simomylodon uccasamamensis* (MNHN-Bol V  
16 3299) in lateral (A), anterior (B), medial (C), posterior (D), proximal (E) and distal (F) views.  
17  
18 Abbreviations: fh, femoral head; gt, greater trochanter; icfo, intercondylar fossa; lco, lateral  
19 condyle; lec, lateral epicondyle; lt, lesser trochanter; mco, medial condyle; mec, medial  
20 epicondyle; pg, patellar groove; tt, third trochanter. Scale bar equals 10 cm.  
21  
22  
23  
24  
25

26 [Suggested size: full page width]  
27  
28  
29  
30

31 **FIG. 10.** Tibia, patella, fibula, and cyamella of the mylodontid sloth *Simomylodon*  
32 *uccasamamensis* (MNHN-Bol V 12518). A-F, right tibia in lateral (A), anterior (B), medial  
33 (C), posterior (D), proximal (E) and distal (F) views; G-H, right patella in anterior (G) and  
34 posterior (H) views; I-L, right fibula in medial (I), lateral (J), posterior (K) and proximal (L)  
35 views; M-N, right cyamella in lateral (M) and articular (N) views. Abbreviations: af,  
36 astragalar facet; atg, anterior tibial groove (for *m. tibialis caudalis*); dff, distal fibular facet;  
37 dif, discoid process facet; dtf, distal tibial facet; fcf, fibular cyamella facet; femf, femoral  
38 facet; fibf, fibular facet; lco, lateral condyle; mco, medial condyle; odf, odontoid process  
39 facet; pff, proximal fibular facet; ptf, proximal tibial facet; ptg, posterior tibial groove; tcf,  
40 tibial cyamella facet; tibf, tibial facet; tt, tibial tuberosity. Scale bar equals 5 cm.  
41  
42  
43  
44  
45  
46  
47  
48  
49  
50  
51  
52  
53

54 [Suggested size: full page width]  
55  
56  
57  
58  
59  
60

1  
2  
3 **FIG. 11.** Left tibia, fibula, and cyamella of the mylodontid sloth *Simomylodon*  
4  
5 *uccasamamensis* (MNHN-Bol V 12518) showing connections among the three elements, in  
6 lateral (A), posterior (B) and proximal (C) views. Scale bar equals 5 cm.  
7  
8

9  
10 [Suggested size: full page width]  
11  
12

13  
14 **FIG. 12.** Calcaneum and astragalus of the mylodontid sloth *Simomylodon uccasamamensis*.  
15

16 A-D, right calcaneum (MNHN-Bol V 8541) in proximal (A), distal (B), lateral (C) and  
17 anterior (D) views; E-H, right astragalus (MNHN-Bol V 12518) in anterior (E), proximal (F),  
18 medial (G) and lateral (H) views. Abbreviations: cn, calcaneal neck; cub, cuboid facet; dif,  
19 discoid facet; ef, ectal facet; ff, fibular facet, navf, navicular facet; odp, odontoid process; st,  
20 sulcus tali; suf, sustentacular facet; tc, tuber calcis; tg, tendinous groove. Scale bar equals 5  
21  
22  
23  
24  
25  
26  
27  
28  
29 cm.

30 [Suggested size: full page width]  
31  
32  
33

34  
35 **FIG. 13.** Tarsal and metatarsal elements of the mylodontid sloth *Simomylodon*  
36

37 *uccasamamensis*. A-C, right navicular (MNHN-Bol V 8541) in distal (A), proximal (B) and  
38 lateral (C) views; D-G, right cuboid (MNHN-Bol V 12518) in dorsal (D), proximal (E), distal  
39 (F) and palmar (G) views; H-I, right ectocuneiform (MNHN-Bol V 12518) in proximal (H)  
40 and distal (I) views; J-N, right metatarsal III (MNHN-Bol V 13495) in dorsal (J), lateral (K),  
41 medial (L), proximal (M) and distal (N) views; O-Q, proximal fragment of right metatarsal  
42 IV (MNHN.F.VIZ28) in proximal (O), lateral (P) and distal (Q) views; R-S, fragment of  
43 metatarsal V (MNHN-Bol V 13450) in proximal (R) and lateral (S) views. Abbreviations  
44 refer to articular facets for the indicated bones, as follows: ast, astragalus, cal, calcaneum;  
45 cub, cuboid; ec/mc, ectocuneiform and mesocuneiform; ect, ectocuneiform; mtt (2-3-4-5),  
46 metatarsal (2-3-4-5); nav, navicular. Scale bar equals 2 cm.  
47  
48  
49  
50  
51  
52  
53  
54  
55  
56  
57  
58  
59  
60

1  
2  
3 [Suggested size: full page width]  
4  
5  
6  
7

8 **FIG. 14.** Dermal ossicles of the mylodontid sloth *Simomylodon uccasamamensis* (MNHN-  
9 Bol V 3726) from the early Pliocene of Casira, Bolivia. Scale bar equals 2 cm.

10  
11  
12 [Suggested size: single column]  
13  
14  
15  
16  
17  
18  
19  
20  
21  
22  
23  
24  
25  
26  
27  
28  
29  
30  
31  
32  
33  
34  
35  
36  
37  
38  
39  
40  
41  
42  
43  
44  
45  
46  
47  
48  
49  
50  
51  
52  
53  
54  
55  
56  
57  
58  
59  
60



Fig. 1. Map of the late Neogene fossil-bearing localities of Bolivia in which the remains of the mylodontid sloth *Simomylodon uccasamamensis* have been recovered. Circles: cities; Stars: fossil localities. [Suggested size: two-thirds page width]

109x109mm (300 x 300 DPI)

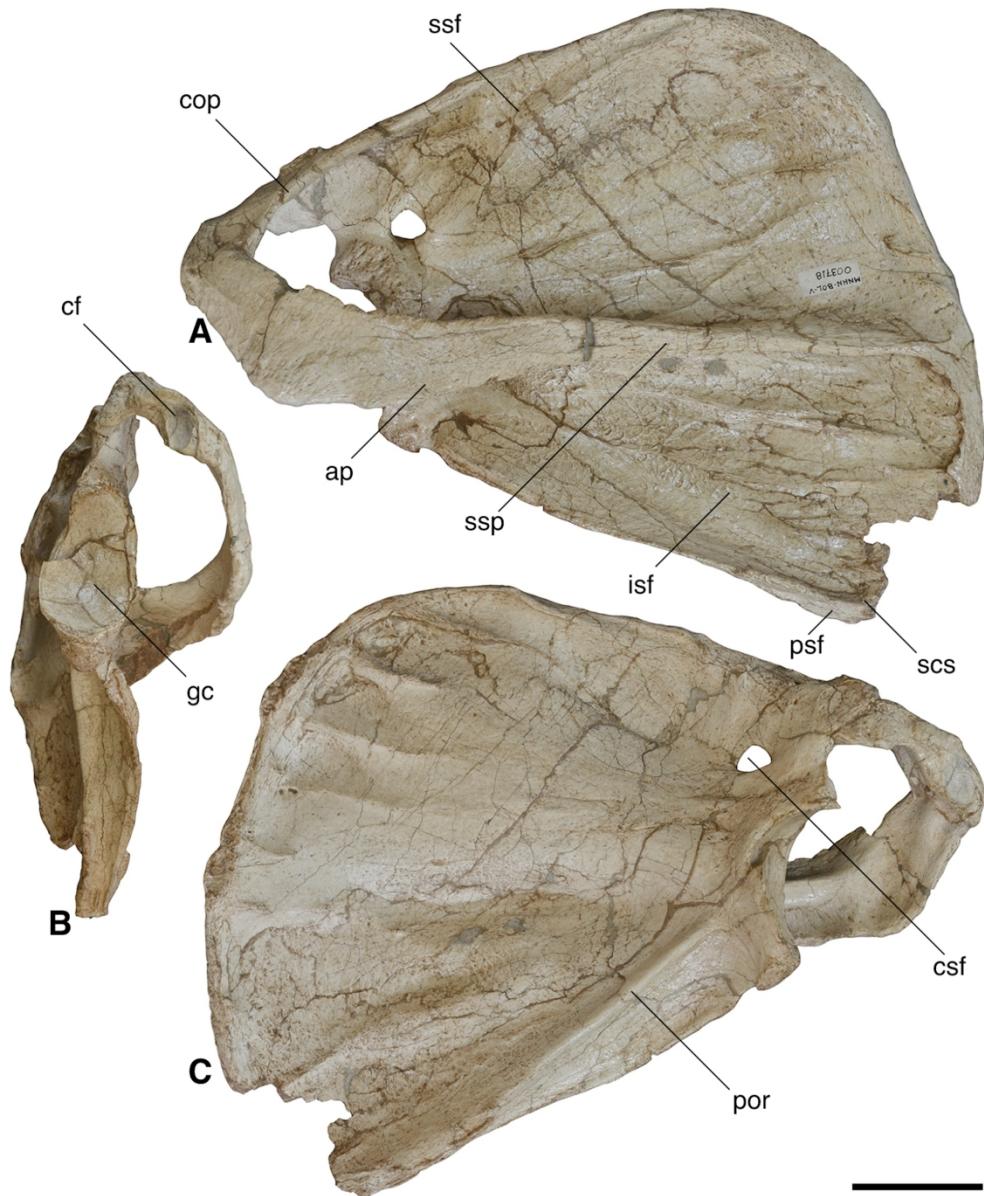


Fig. 2. Left scapula of the mylodontid sloth *Simomylodon uccasamamensis* (MNHN-Bol V 3718) in lateral (A), proximal (B) and medial (C) views. Abbreviations: ap, acromion process; cf, clavicular fossa; cop, coracoid process; csf, coraco-scapular foramen; gc, glenoid cavity; isf, infraspinous fossa; por, posterior ridge of subscapular fossa; psf, post-scapular fossa; scs, secondary spine; ssf, supraspinous fossa; ssp, spine of scapula. Scale bar equals 5 cm.

109x134mm (600 x 600 DPI)

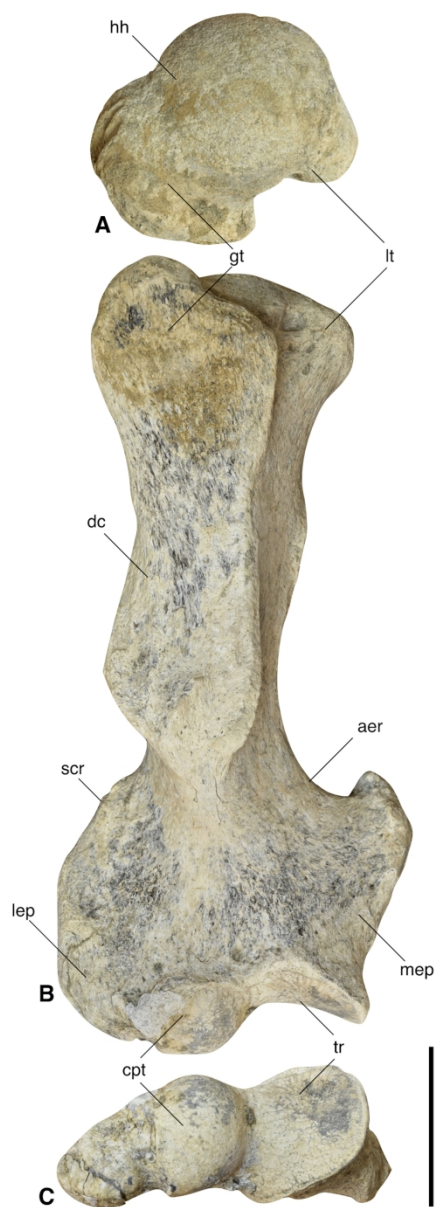


Fig. 3. Right humerus of the mylodontid sloth *Simomylodon uccasamamensis* (MNHN-Bol V 13367) in proximal (A), anterior (B) and distal (C) views. Abbreviations: aer, ascending entepicondylar ridge; cpt, capitulum; dc, deltoid crest; gt, greater tuberosity; hh, humeral head; lep, lateral epicondyle; lt, lesser tuberosity; mep, medial epicondyle; scr, supinator crest, tr, trochlea. Scale bar equals 5 cm.

80x223mm (600 x 600 DPI)



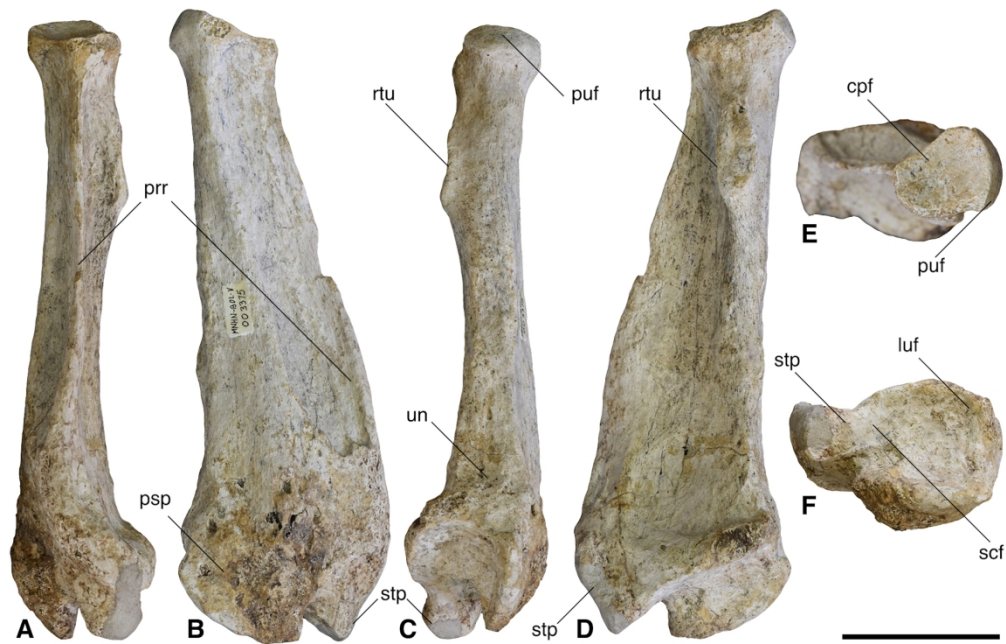


Fig. 4. Right radius of the mylodontid sloth *Simomylodon uccasamamensis* (MNHN-Bol V 3375) in anterior (A), lateral (B), posterior (C), medial (D), proximal (E) and distal (F) views. Abbreviations: cpf, capitular facet; luf, lunar facet; psp, pseudostyloid process; prr, pronator ridge; puf, proximal ulnar facet; rtu, radial tuberosity; scf, scaphoid facet; stp, styloid process; un, ulnar notch. Scale bar equals 5 cm.

165x105mm (600 x 600 DPI)

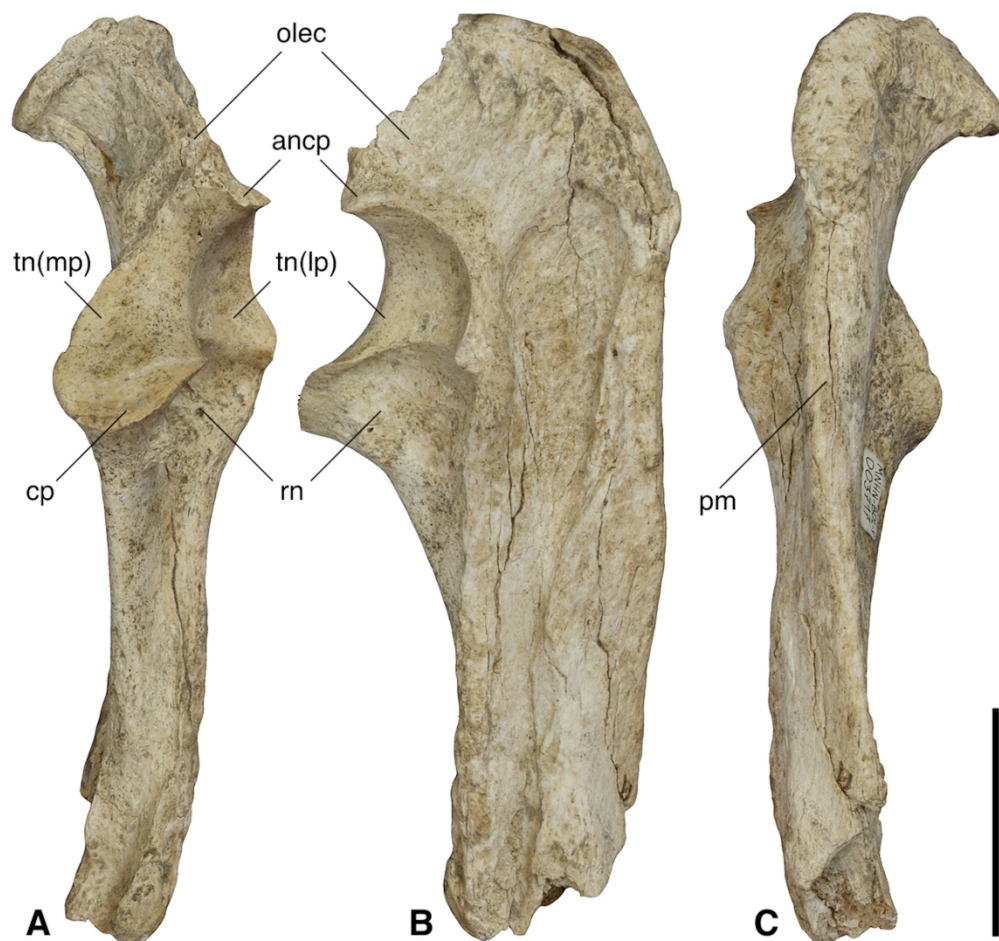


Fig. 5. Proximal fragment of left ulna of the mylodontid sloth *Simomylodon uccasamamensis* (MNHN-Bol V 3717) in anterior (A), lateral (B) and posterior (C) views. Abbreviations: ancp, anconeal process; cp, coronoid process; olec, olecranon; pm, posterior margin; rn, radial notch; tn(lp), trochlear notch (lateral portion); tn(mp), trochlear notch (medial portion). Scale bar equals 5 cm.

109x103mm (600 x 600 DPI)

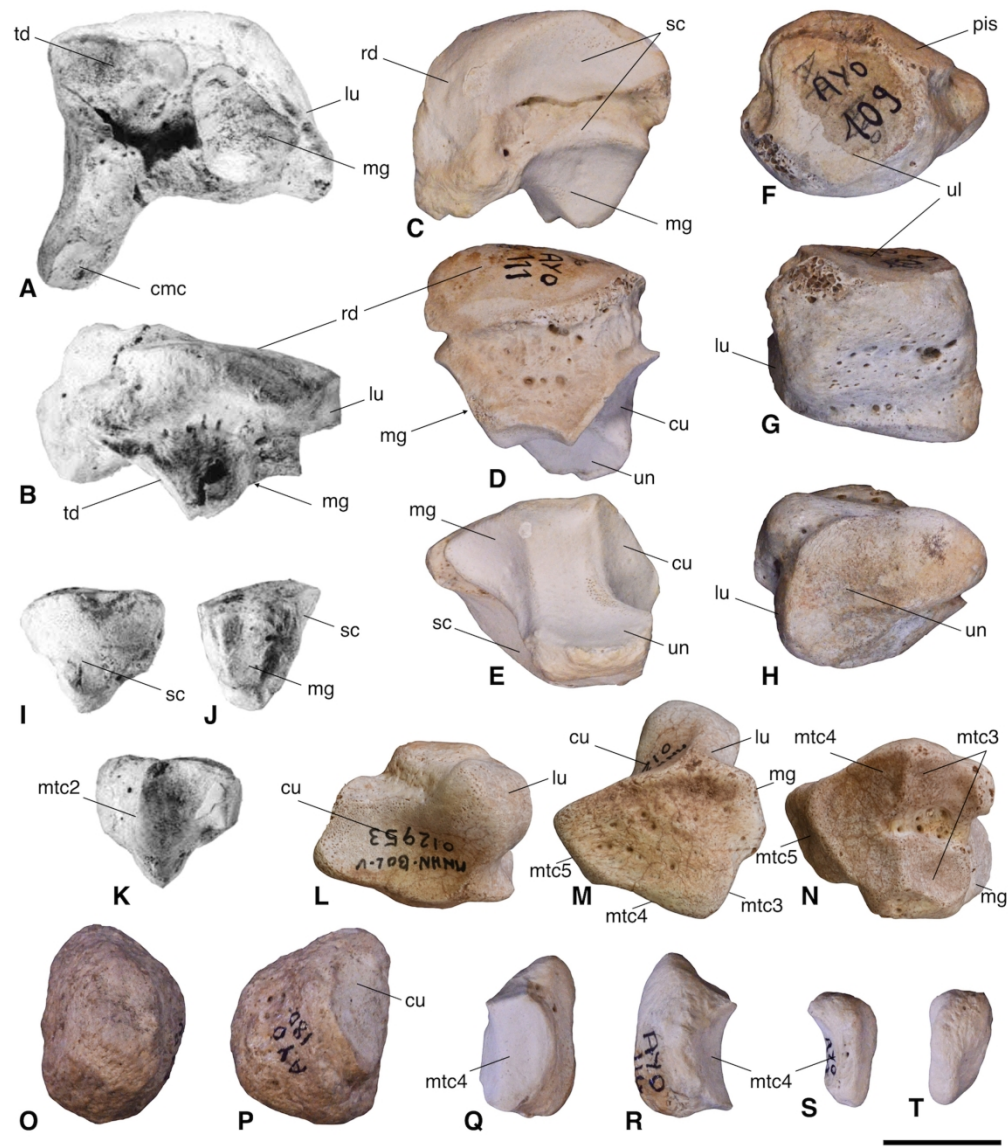


Fig. 6. Carpals (A-P) and sesamoids (Q-T) of the mylodontid sloth *Simomylodon uccasamamensis*. A-B, left scaphoid (MNHN.F.AYO180) in distal (A) and dorsal (B) views; C-E, left lunar (MNHN.F.AYO111) in anterior (C), dorsal (D) and distal (E) views; F-H, left cuneiform (MNHN.F.AYO109) in proximal (F), dorsal (G) and distal (H) views; I-K, left trapezoid (MNHN.F.AYO180) in proximal (I), posterior (J) and distal (K) views; L-N, right unciform (MNHN-Bol V 12953) in proximal (L), dorsal (M) and distal (N) views; O-P, right pisiform (MNHN.F.AYO180) in palmar (O) and oblique-palmar (P) views; Q-R, right medial sesamoid of mtc4 (MNHN.F.AYO114) in medial (Q) and lateral (R) views; S-T, right lateral sesamoid of mtc4 (MNHN.F.AYO111) in medial (S) and palmar (T) views. Black and white photos have been taken from St-André et al. (2010). Abbreviations refer to articular facets for the indicated bones, as follows: cmc, carpal-metacarpal complex; cu, cuneiform, lu, lunar; mg, magnum; mtc (2-3-4-5), metacarpal (2-3-4-5); pis, pisiform; rd, radius; sc, scaphoid; td, trapezoid; ul, ulna; un, unciform. Scale bar equals 2 cm.

165x189mm (600 x 600 DPI)





Fig. 7. Metacarpal elements of the mylodontid sloth *Simomylodon uccasamamensis*. A-B, right carpal-metacarpal complex (MNHN.F.VIZ32) in dorsal (A) and distal (B) views; C-E, right metacarpal II (MNHN.F.AYO190) in anterior (C), posterior (D) and proximal (E) views; F-H, right metacarpal III (MNHN.F.VIZ27) in dorsal (F), palmar (G) and proximal (H) views; I-M, left metacarpal III fused with magnum (MNHN.F.AYO179) in proximal (I), dorsal (J), posterior (K), palmar (L) and anterior (M) views; N-P, proximal fragment of left metacarpal IV (MNHN.F.VIZ33) in proximal (N), dorsal (O) and posterior (P) views; Q-S, left metacarpal V (MNHN-Bol V 13367) in anterior (Q), dorsal (R) and distal (S) views. Abbreviations refer to articular facets for the indicated bones, as follows: cmc, carpal-metacarpal complex; lu, lunar; mg, magnum; mtc (2-3-4-5), metacarpal (2-3-4-5); pp (1-2-3-5), proximal phalanx (1-2-3-5); sc, scaphoid; td, trapezoid; un, unciform. Scale bar equals 2 cm.

165x241mm (600 x 600 DPI)

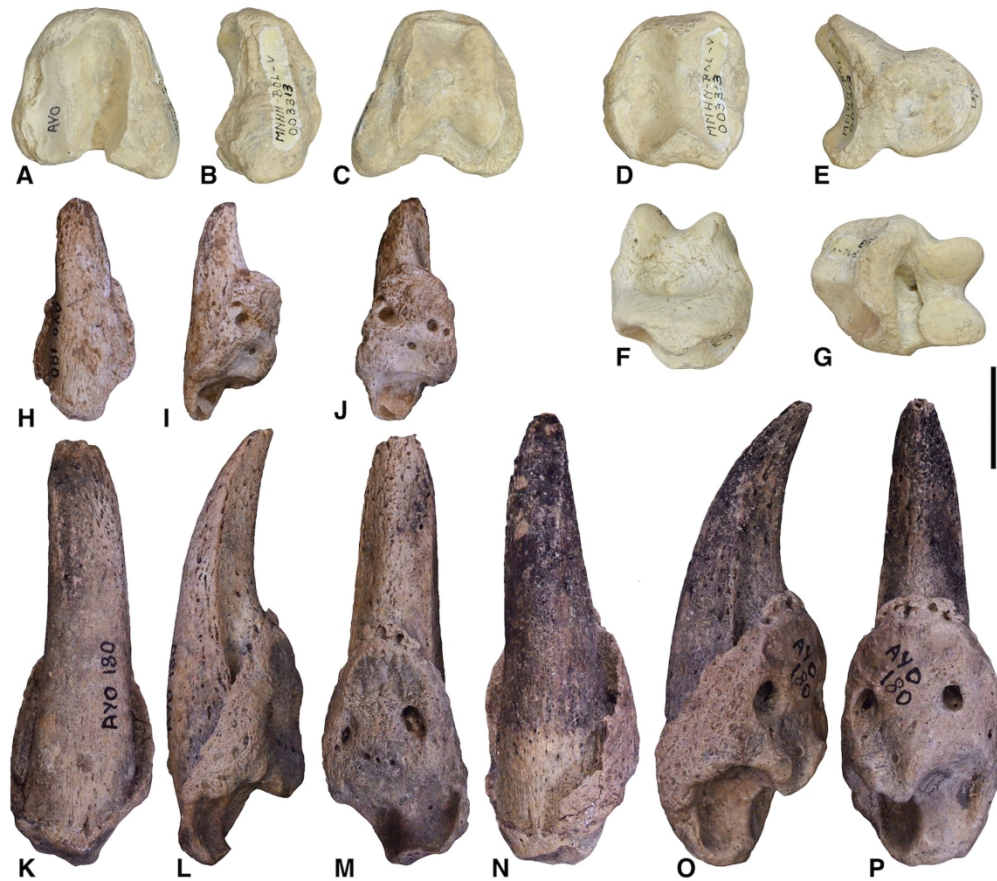


Fig. 8. Manual phalanges of the mylodontid sloth *Simomylodon uccasamamensis*. A-C, right proximal phalanx of third digit (MNHN-Bol V 3313) in proximal (A), lateral (B) and distal (C) views; D-G, right intermediate phalanx of third digit (MNHN-Bol V 3313) in proximal (D), lateral (E), dorsal (F) and palmar (G) views; H-J, left ungual phalanx of first digit (MNHN.F.AYO180) in dorsal (H), medial (I) and palmar (J) views; K-M, left ungual phalanx of second digit (MNHN.F.AYO180) in dorsal (K), medial (L) and palmar (M) views; N-P, left ungual phalanx of third digit (MNHN.F.AYO180) in dorsal (N), medial (O) and palmar (P) views. Scale bar equals 2 cm.

165x145mm (600 x 600 DPI)

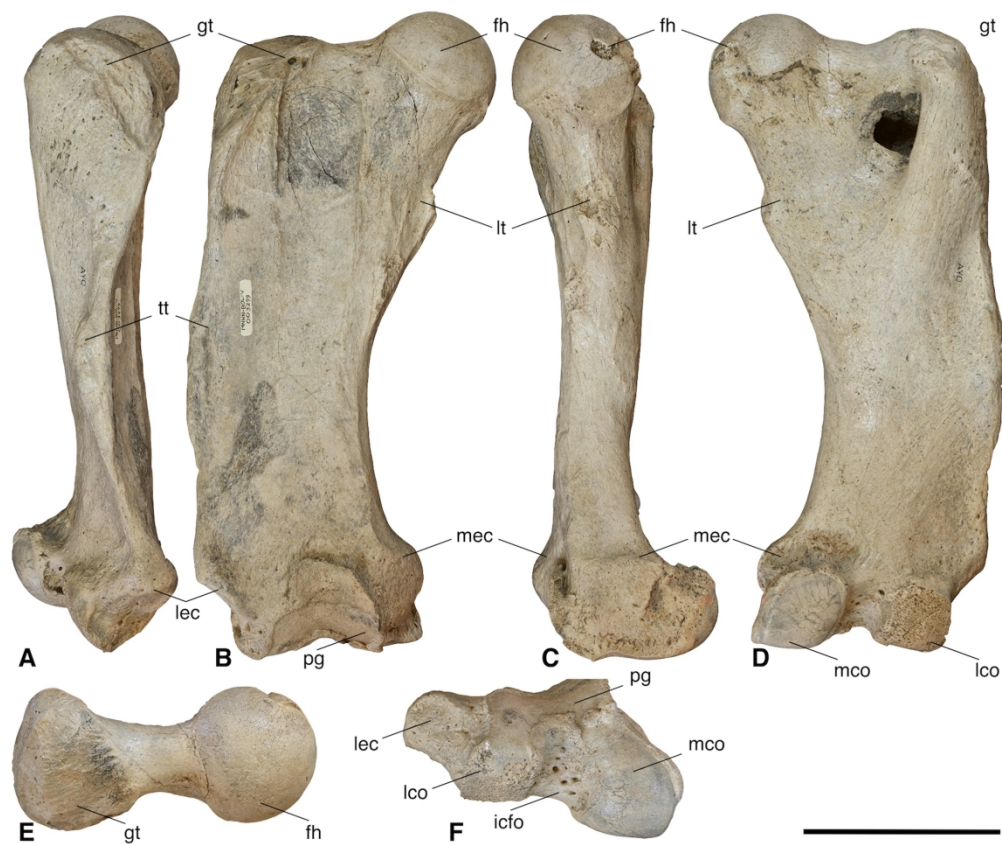


Fig. 9. Right femur of the mylodontid sloth *Simomylodon uccasamamensis* (MNHN-Bol V 3299) in lateral (A), anterior (B), medial (C), posterior (D), proximal (E) and distal (F) views. Abbreviations: fh, femoral head; gt, greater trochanter; icfo, intercondylar fossa; lco, lateral condyle; lec, lateral epicondyle; lt, lesser trochanter; mco, medial condyle; mec, medial epicondyle; pg, patellar groove; tt, third trochanter. Scale bar equals 10 cm.

165x138mm (600 x 600 DPI)





Fig. 10. Tibia, patella, fibula, and cyamella of the mylodontid sloth *Simomylon uccasamamensis* (MNHN-Bol V 12518). A-F, right tibia in lateral (A), anterior (B), medial (C), posterior (D), proximal (E) and distal (F) views; G-H, right patella in anterior (G) and posterior (H) views; I-L, right fibula in medial (I), lateral (J), posterior (K) and proximal (L) views; M-N, right cyamella in lateral (M) and articular (N) views.

Abbreviations: af, astragalar facet; atg, anterior tibial groove (for *m. tibialis caudalis*); dff, distal fibular facet; dif, discoid process facet; dtf, distal tibial facet; fcf, fibular cyamella facet; femf, femoral facet; fibf, fibular facet; lco, lateral condyle; mco, medial condyle; odf, odontoid process facet; pff, proximal fibular facet; ptf, proximal tibial facet; ptg, posterior tibial groove; tcf, tibial cyamella facet; tibf, tibial facet; tt, tibial tuberosity. Scale bar equals 5 cm.

165x166mm (600 x 600 DPI)



Fig. 11. Left tibia, fibula, and cymella of the mylodontid sloth *Simomylon uccasamamensis* (MNHN-Bol V 12518) showing connections among the three elements, in lateral (A), posterior (B) and proximal (C) views. Scale bar equals 5 cm.

165x46mm (600 x 600 DPI)



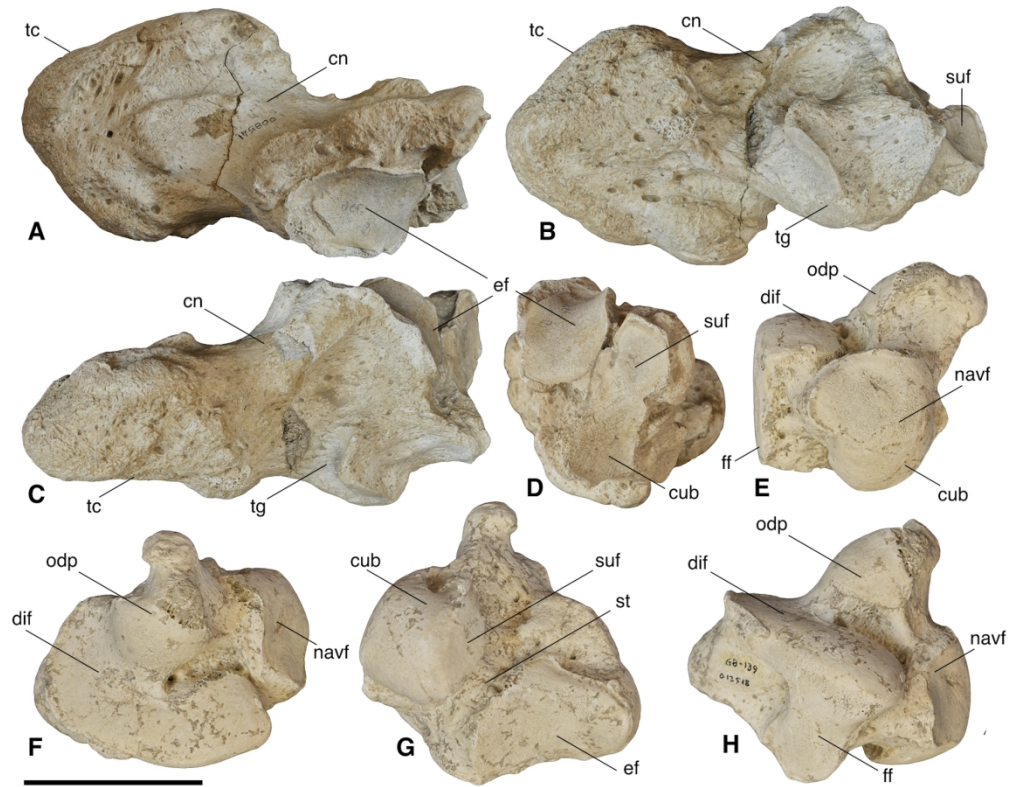


Fig. 12. Calcaneum and astragalus of the mylodontid sloth *Simomylodon uccasamamensis*. A-D, right calcaneum (MNHN-Bol V 8541) in proximal (A), distal (B), lateral (C) and anterior (D) views; E-H, right astragalus (MNHN-Bol V 12518) in anterior (E), proximal (F), medial (G) and lateral (H) views. Abbreviations: cn, calcaneal neck; cub, cuboid facet; dif, discoïd facet; ef, ectal facet; ff, fibular facet, navf, navicular facet; odp, odontoid process; st, sulcus tali; suf, sustentacular facet; tc, tuber calcis; tg, tendinous groove. Scale bar equals 5 cm. [Suggested size: full page width]

165x130mm (300 x 300 DPI)

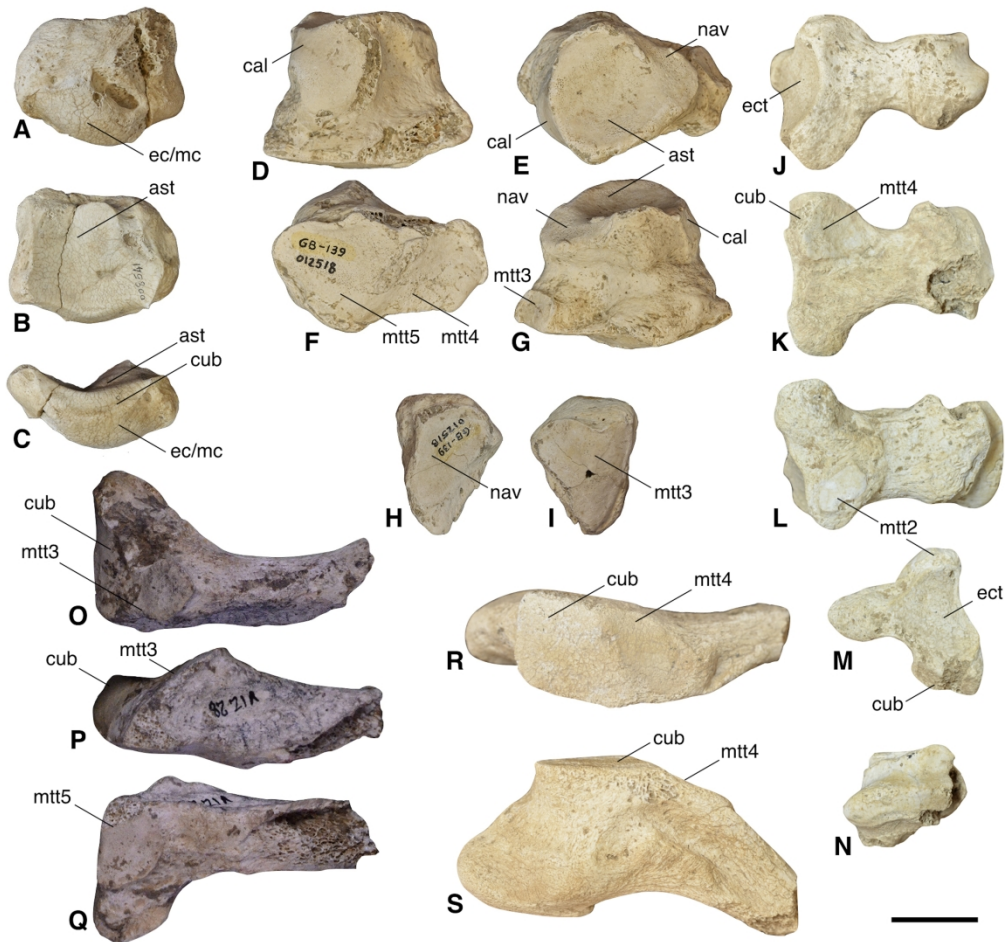


Fig. 13. Tarsal and metatarsal elements of the mylodontid sloth *Simomylodon uccasamamensis*. A-C, right navicular (MNHN-Bol V 8541) in distal (A), proximal (B) and lateral (C) views; D-G, right cuboid (MNHN-Bol V 12518) in dorsal (D), proximal (E), distal (F) and palmar (G) views; H-I, right ectocuneiform (MNHN-Bol V 12518) in proximal (H) and distal (I) views; J-N, right metatarsal III (MNHN-Bol V 13495) in dorsal (J), lateral (K), medial (L), proximal (M) and distal (N) views; O-Q, proximal fragment of right metatarsal IV (MNHN.F.VIZ28) in proximal (O), lateral (P) and distal (Q) views; R-S, fragment of metatarsal V (MNHN-Bol V 13450) in proximal (R) and lateral (S) views. Abbreviations refer to articular facets for the indicated bones, as follows: ast, astragalus, cal, calcaneum; cub, cuboid; ec/mc, ectocuneiform and mesocuneiform; ect, ectocuneiform; mtt (2-3-4-5), metatarsal (2-3-4-5); nav, navicular. Scale bar equals 2 cm.

165x156mm (600 x 600 DPI)

1  
2  
3  
4  
5  
6  
7  
8  
9  
10  
11  
12  
13  
14  
15  
16  
17  
18  
19  
20  
21  
22  
23  
24  
25  
26  
27  
28  
29  
30  
31  
32  
33  
34  
35  
36  
37  
38  
39  
40  
41  
42  
43  
44  
45  
46  
47  
48  
49  
50  
51  
52  
53  
54  
55  
56  
57  
58  
59  
60



Fig. 14. Dermal ossicles of the mylodontid sloth *Simomylodon uccasamamensis* (MNHN-Bol V 3726) from the early Pliocene of Casira, Bolivia. Scale bar equals 2 cm.

80x51mm (600 x 600 DPI)